Power System Technology
ISSN:1000-3673

Received: 16-01-2024 Revised: 12-02-2024 Accepted: 07-03-2024

Prioritization of Watershed Flooding Using the TUFLOW Hydrological Model and FRI-EO_Learn Smart Method

Amir Sheikhzadeh Asadi[1], Navid Jalalkamali[*2], Amir Robati[3]

1. PhD student, Department of Civil Engineering, Kerman Branch, Islamic Azad University, Kerman, Iran. Email address:Amirsheikhzadehapple@gmail.com
2. Assistant Professor, Department of Water Sciences and Engineering, Kerman Branch, Islamic Azad University, Kerman, Iran. Email address:Njalalkamali@iauk.ir
3. Assistant Professor, Department of Civil Engineering, Kerman Branch, Islamic Azad University, Kerman, Iran. Email address:Ammirrr@hotmail.com

Abstract

The effects of human activities and climate changes, which appear in the form of changes in the vegetation of desert areas, or agricultural fields in semi-arid climates, can change the nature of flood propagation downstream, especially in the urban areas of a basin. Drainage should be effective. In this study, in order to extract rainfall-flood relationships in an urban area of Vahdatiyeh, the sum of hydrological relationships as well as numerical and hydraulic models were used until the use of vulnerability index and zoning. By examining the question of whether the changes in the volume and form of flood propagation in an urban catchment basin can reduce part of the infiltration of water into the soil by changing the shape, speed and depth of the flow in the river network of that basin, which Following the development of impervious surfaces of urban use or soils with minimal vegetation in the upstream flood basin (increasing the runoff coefficient), should it compensate? The hypothesis of this study is based on this model that increasing the water level in the rivers, as long as the water level in the aquifer is lower than the height of the river bed, has no effect on the amount of infiltration from the river into the soil. Extraction of the volume and type of flow distribution in the upstream of Vahdatiyeh city, which is the center of flood entry from two waterway branches, was done by the method of regional analysis and the extraction of floods with a historical and at the same time probable return period. The TUFLOW numerical model was used to prepare the basic flow simulator. In order to prepare a structure for determining sensitive areas in flooding, from the processing of hundreds of Sentinel-2 satellite images for the period from 2016 to 2021 in preparing the NDWI index as a standardized measure of changes in water structures as well as land cover, and a detailed geological layer on Machine learning method and EO method were used as the basis of classification. The land structure layer was chosen as the criteria for classifying areas in determining the priority of flood risk. With the assumption that the increase in nutrition will be done only if the flood channels expand in a historical event. In this way, in this study, from the equations for determining water losses, under the title SCS-CN with a

Power System Technology
ISSN:1000-3673

Received: 16-01-2024 Revised: 12-02-2024 Accepted: 07-03-2024

cumulative distribution function for limiting conditions, the amount of water storage capacity in the soil at the basin level, using standard layers of depth and impermeability in Two possible conditions of a similar flood were implemented, and we calculated with different flow loss figures. Determining and separating the effect of the effective range of feeding and losses in this method was done using a three-dimensional model with 22 vertical layers of MODFLOW code. The results of this research show that to determine flood-prone areas, the basic criterion should be the geological diversity in the simultaneous analysis with the agricultural development of the region. Using the images of sentinel satellites, it is possible to determine the classified intervals to receive the most changes in the NDWI index. These spatial intervals better determine the decision-making limits for the implementation of flow diversion structures, and even the limits of cultivation in order to restore the climate against droughts resulting from agriculture. In the upstream of Vahdatiye city, the elevation zone number 1 of the land structure class, which is in direct contact with the urban area and the flood-prone area, does not show the figures and numbers resulting from vegetation changes at least in the 5-year period. The reason for this issue can be explained by the agricultural activities in this area, or at least the fact that the mentioned area is downstream to receive surface water resources. But the scattered parts of the east are considered to be the main cause of the flood. In other words, unstructured agriculture has been effective in flooding the steep and higher areas of the study catchment area. Therefore, in the implementation of flood control plans, priority should be given to this part of the coordinate boundaries. Also, the results show that there are 2,831 man-made user units in the first class at a distance of 100 meters from the floodplain in Vahdatiye city. The first class specifies residential and commercial units.

Keywords: urban flooding, machine, EO method, TUFLOW, Soil Wetting

Introduction

According to the outlook of the OECD environment organization, the number of extreme weather events will increase worldwide by 2050 (Organization for Economic Co-operation and Development, 2012). A large number of studies show that climate change leads to a 27-fold increase in the frequency and intensity of abnormal weather events (IPCC, 2014; Aalbers et al, 2018; Martel et al, 2019; Sillmann et al, 2013; Fischer, 2016 and Knutti). Recent data from the Center for Research on the Epidemiology of Disasters shows that floods accounted for more than 47% of all weather-related disasters in the period from 1995 to 2015, as reported by the Center for Research on Epidemiology of Disasters (CRED) United Nations Office for Disaster Risk Reduction (UNISDR, 2015). Population growth and uncontrolled construction in flood plains are two factors that increase vulnerability to extreme weather events. Despite increasing global awareness, as shown by several reports of the World Bank, IPCC, the European Commission and the United Nations in 2013 and 2014, moving towards flood-resilient cities remains a major challenge in developing countries and has been developed (Vis et al, 2003). This transition to a flexible approach (focused on flexible and adaptive solutions) clearly requires a departure from the traditional resistance-based approach (focused on flood-safe

Power System Technology
ISSN:1000-3673
Received: 16-01-2024 Revised: 12-02-2024 Accepted: 07-03-2024

solutions) in flood risk management (Tempels and Hartmann, 2014). Therefore, it can be considered with certainty that urban areas all over the world are increasingly exposed to surface water flooding due to rapid urbanization, installation of complex infrastructures and changes in precipitation patterns caused by human climate changes. (Willems et al, 2012). For example, Hammond et al. (2015) showed recent surface water flood events in Brisbane in January 2011, in Bangkok in the 2011 monsoon season, and in Beijing in July 2012. When impacts can be significant, with disruption of services, damage to critical infrastructure and assets, as well as other societal impacts with regard to future projections of population, urbanization and human climate change. , such incidents will probably intensify. The Intergovernmental Panel on Climate Change (IPCC, 2014) has emphasized with high confidence that it is predicted that in urban areas, climate change will increase risks for people, property, economy and ecosystems, including the risks caused by heavy rainfall. will be.

The risk of surface water flooding (sometimes known as "urban" flooding or "storm water") emerges from the interaction between biophysical and human factors (Hall et al, 2003). Biophysical factors determine the frequency, duration and intensity of rainfall and runoff that occurs when rain hits the ground. Rain may penetrate the ground, but in urban areas with an impermeable surface, the rain changes in directions that are modified by the form of buildings and streets and accumulates in places with low topographic height. . These processes are modified by drains designed to transport water away from urban areas on the surface or in pipes (Blanc et al, 2012). The risk also depends on the vulnerability of the area and population exposed to this event (Hall et al, 2005) and the effectiveness of surface water management interventions.

TUFLOW model

TUFLOW is a powerful computational engine that provides one-dimensional and two-dimensional solutions of the free surface flow equations for simulating flood propagation and tidal wave propagation. TUFLOW also provides a flood modeling solution by seamlessly coupling one-dimensional and two-dimensional state flow (transforming flows). and advances calculations in flexible, robust conditions and in a wide range of features that no other product offers. TUFLOW is suitable for modeling in the following conditions:

• Flooding of rivers and streams with complex flow patterns

• Piped areas in urban areas

• River hydraulics and coastal tides

• Analysis of storm tides and tsunamis

TUFLOW computing model works in harmony with GIS software such as MapInfo or SAGA or through the Aquaveo SMS user interface. TUFLOW is originally the product of a joint research and development project between WBM Pty Ltd and the University of Queensland,

Power System Technology
ISSN:1000-3673
Received: 16-01-2024 Revised: 12-02-2024 Accepted: 07-03-2024

which was completed in 1990. By 1997 it was widely used by WBM Pty Ltd for river studies and flood study applications. Since 1997, significant advances have been made in flood modeling capabilities and GIS linkages, leading to widespread use for flood research worldwide. TUFLOW's 2D solution is based on Stelling's finite difference grid, which solves the 2D free surface shallow water flow equations. This design has been improved to handle upstream flow control regimes (eg supercritical flow), bridge decks, beds and other features. The widely applicable one-dimensional solution based on WBM software solves the Saint-Venant equations using an explicit two-step solution.

TUFLOW continues to improve and evolve to solve hydrodynamic modeling challenges. Its strengths are:

• Quick and stable wet and dry mode;

• Linking one-dimensional and two-dimensional flow

• Multiple two-dimensional domains (optional).

• Both one-dimensional and two-dimensional flow representations of hydraulic structures.

• Automatic upstream/downstream controlled flow regime switching.

• One-dimensional and two-dimensional supercritical flow.

• Very flexible and efficient data processing.

• based on GIS; And

• Extensive quality control outputs.

TUFLOW became commercially available in 2001. Its popularity has been greatly expanded by the recommendations of users. Larger organizations, even global organizations with other similar products in their possession, quickly realized that the performance of TUFLOW licenses is much more powerful. The TUFLOW interface in SMS can be used to build TUFLOW models and view and analyze the results.

Some features of the user interface are:

• Creates two-dimensional ranges from bathymetry grid data.

• Extracts one-dimensional cross-sectional areas from TIN data.

• Defines one-dimensional pipe domains, including connections to surfaces.

• Imports data from ArcGIS or MapInfo formats.

• Defines boundary conditions in one-dimensional nodes, two-dimensional lines or two-dimensional polygons.

Power System Technology
ISSN:1000-3673
Received: 16-01-2024 Revised: 12-02-2024 Accepted: 07-03-2024

• Creates two-dimensional geometric changes to model objects such as variable boundaries.

• Calculates material properties such as Manning's n and hydrological losses.

• Separates simulations from high-rise building blocks.

• Simulations share common data to avoid data duplication errors and make it easy to update the project with new data.

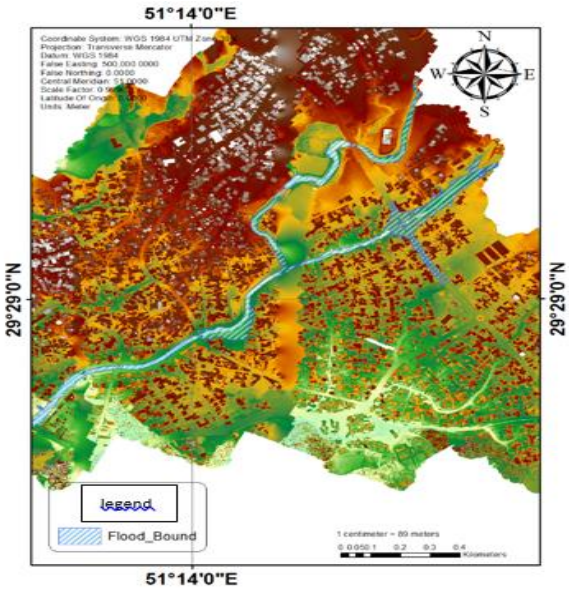

Figure 2. Real flood zone on the elevation .model of the city

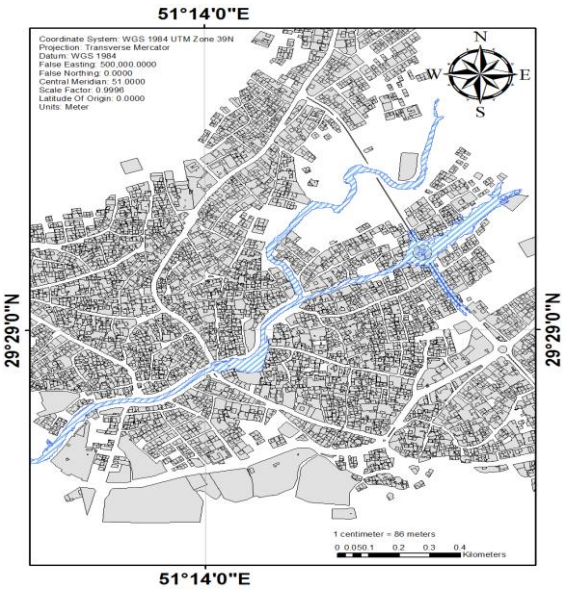

Figure 1. Real flood protection in the city .limits

Figures (1) and (2) show the area of the flood event in its largest state in the urban area as the output of the hydraulic model. The first picture shows the structural structure of the city and the second picture shows the changes in the digital model of the height for this flood zone. An important point in urban flooding is the non-linear process of regional vulnerability. This means that if a passage is blocked due to flooding due to the collapse of a dilapidated structure, this situation will eventually lead to a crisis in a number of structures around that building. Therefore, although the rising water in its primitive form affects a unique and specific area, but with the extension of the critical process and the prolongation of the secondary events, this situation can even lead to the blockage of the sewage transmission network in terms of personal health. And the water cut and... should be intensified.

In forms (4) to (9), the structures that are located at a significant distance from the flood event are separated by a certain limit. These distances were equivalent to 0, 5, 10, 25, 50, and 100 meters. Although the 100 meter distance of structures and buildings are not necessarily directly exposed to flooding, however, according to what was mentioned in the previous paragraph, the

Power System Technology
ISSN:1000-3673
Received: 16-01-2024 Revised: 12-02-2024 Accepted: 07-03-2024

limited access and infrastructure dependence of each area can be several times the direct distance according to experience. Involve the flood with the crisis of this natural event. The greater the distance, the less the severity of the crisis, however, this risk does not necessarily decrease with the increase of the distance. Also, Figure (3) shows the guide for each image of the mentioned boundaries.

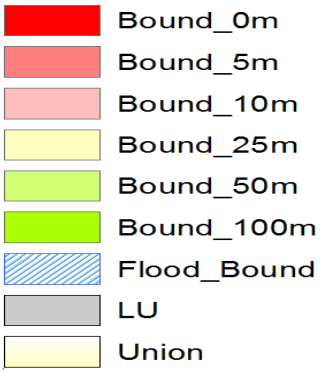

Figure 3. Guide to images of flood protection.

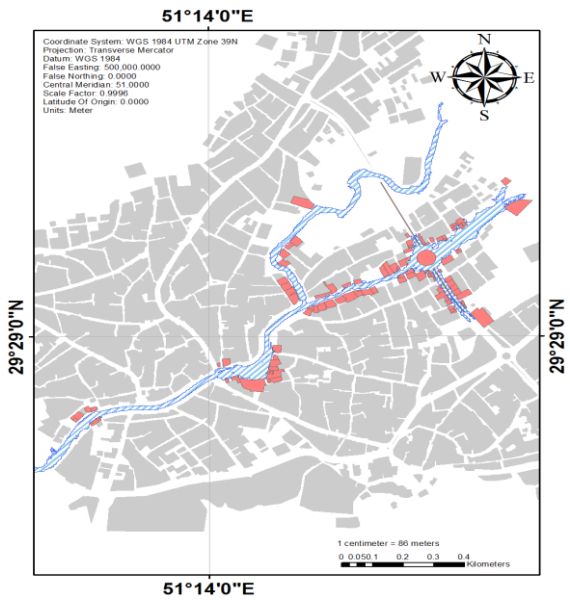

Figure 5. The distance of five meters from .the flood

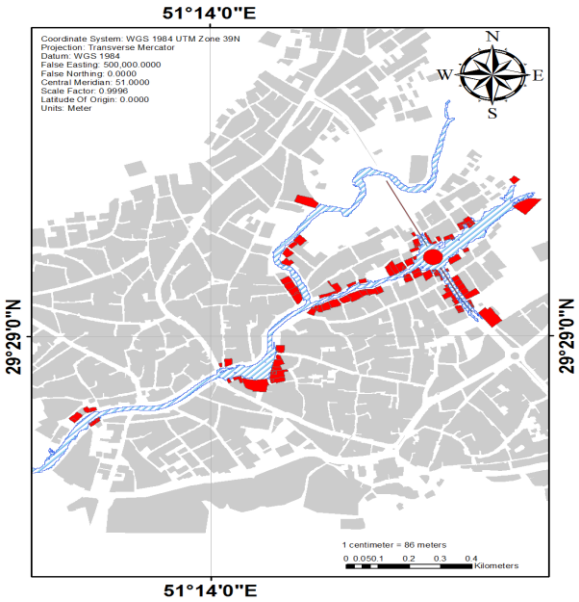

Figure 4. Harem without distance from .floods

Power System Technology
ISSN:1000-3673

Received: 16-01-2024 Revised: 12-02-2024 Accepted: 07-03-2024

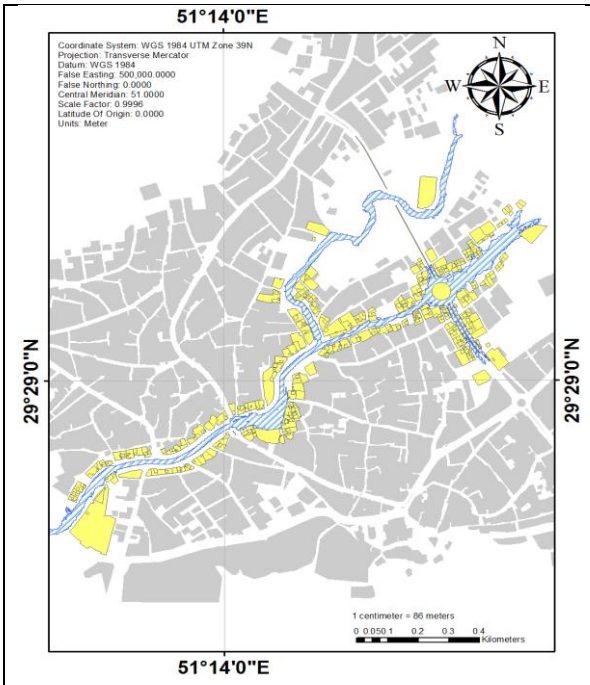

Figure 7. The distance of 25 meters from .the flood

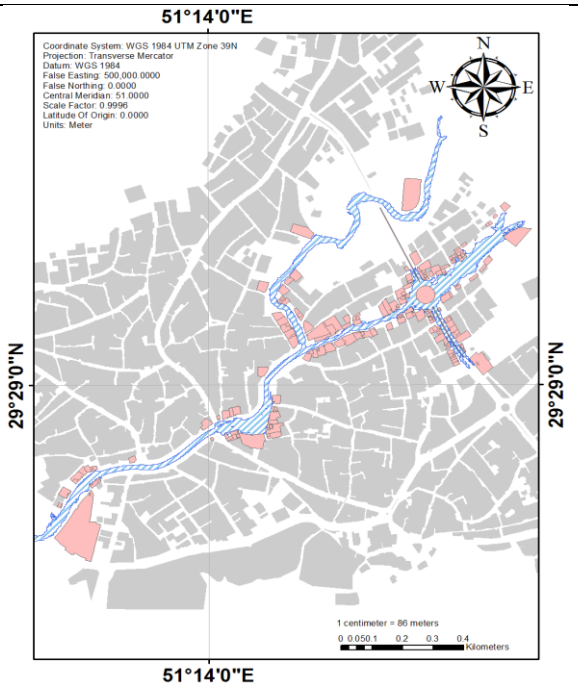

Figure 6- The distance of 10 meters from the .flood

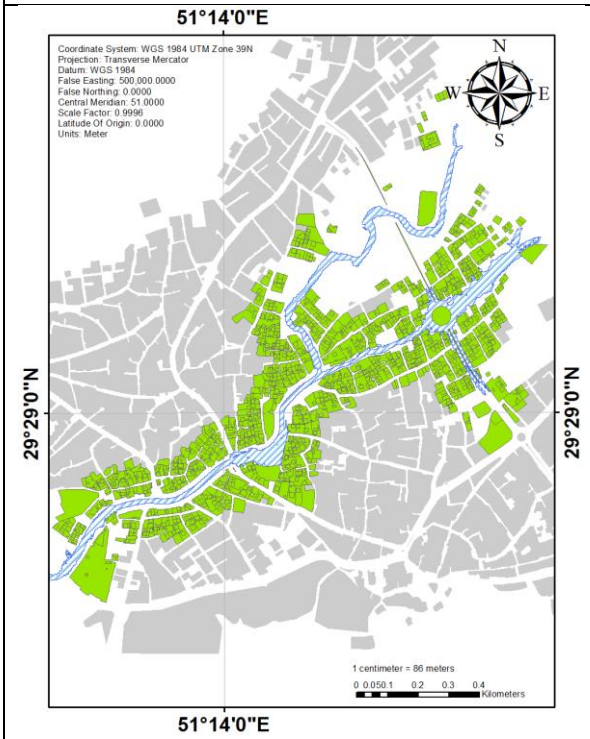

Figure 9. The distance of 100 meters from .the flood

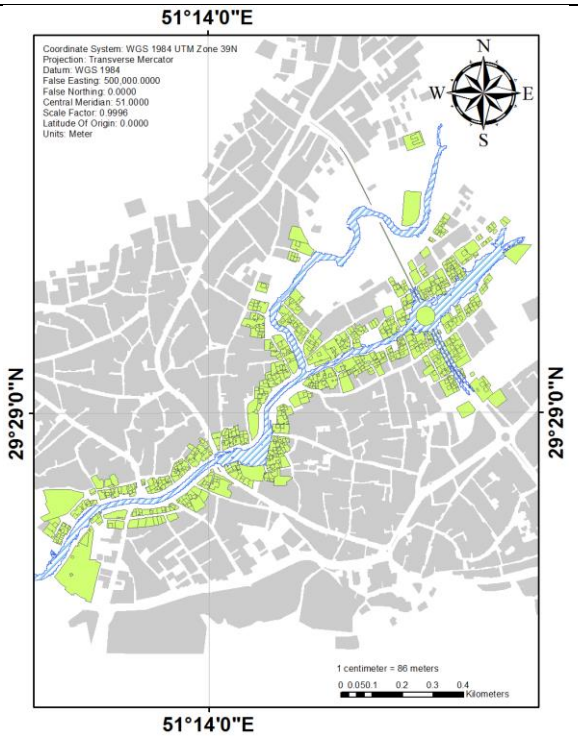

Figure 8. The distance of 50 meters from the .flood

Power System Technology
ISSN:1000-3673
Received: 16-01-2024 Revised: 12-02-2024 Accepted: 07-03-2024

In figures (4) to (9), the red areas show structures and buildings that are directly exposed to apple damage. These structures actually deal with the rainfall that has a return period of 50 years. This collision can also lead to the announcement of the danger of collapse if worn out structures are identified. But the areas marked with green color will not directly deal with flood flows. At the same time, they will be involved with the crisis indirectly compared to other city areas marked with gray color. The privacy set here is specified using the geographic information system command and the digits assigned to the privacy according to the upper hand position of the vulnerability index layer.

Table 1. Statistical summary of the computational domain of urban area flood damage index.

The amount of privacy	**The total area in the sanctuary Square) (meters**	**environment in privacy (Meter)**	**First class user**	**Second class user**	**Third class user**
zero meters	55536.445	16893.271	243	9	2
five meters	55536.445	16893.271	243	9	2
ten meters	114850.416	24363.922	376	11	2
Twenty five meters	198752.885	48243.675	891	17	2
fifty meters	322233.222	79185.381	1570	24	2
one hundred meters	562567.524	138997.542	2831	45	2

According to table (1), the number of structures increases naturally as the distance from the flood zone increases. This has followed the experience of flood risk development. But with the passage of time, generally, the hydrological dry periods that dominate an area for a long time, make the process of urban development completely unsustainable. In the city of Vahdatieh, there are 2831 man-made user units, which are in the first class, at a distance of 100 meters from the flood zone. The first class specifies residential and commercial units. The second class, which shows the number of 45 numbers, is non-residential areas, and the constant number 2 at different intervals for class number 3 determines the position of waterways and canals. While the normal 5-year flood with 243 user classes is certain, the increasing trend of the slope distance indicates a slower increase in the number of structures at risk. This means that the occurrence of floods with a return period of 100 years or more or in worse conditions will lead to a serious situation. Another important point is that the amount of changes in the area with the change in the distance from the flood has a slower growth rate than the number of structures. This means a higher density by moving away from the waterway, which confirms the recent analysis.

Power System Technology
ISSN:1000-3673
Received: 16-01-2024 Revised: 12-02-2024 Accepted: 07-03-2024

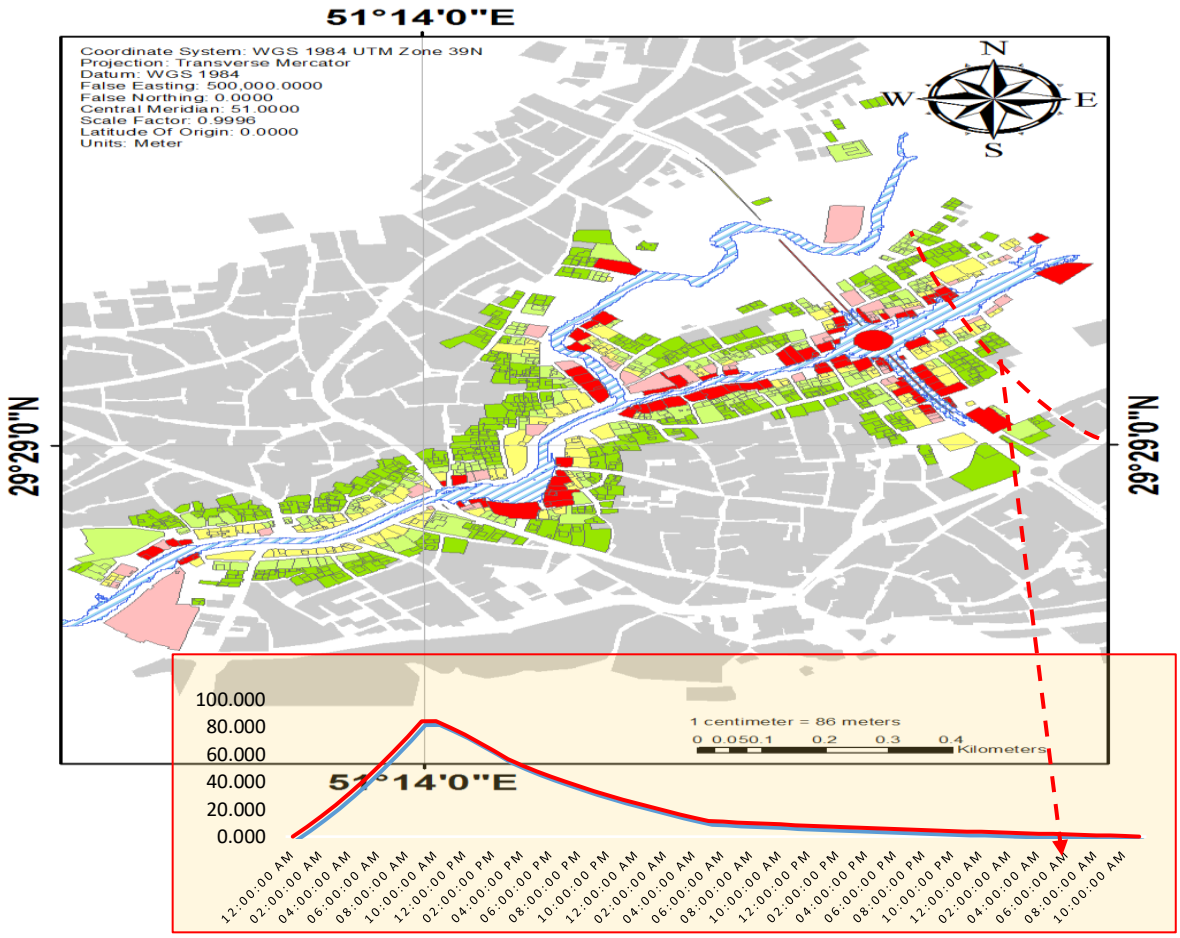

Figure 10. Flood risk index map in Vahdatieh urban area.

Figure (10) shows the location of the urban area and especially the flood channel that is affected by the flood event. The areas with red color are under direct risk, the areas with yellow color are under indirect risk but with a high degree of risk, and the areas with pale green color and then deep green are under indirect risk and with a lower degree of risk. Factors that can potentially make the existing situation in the city more critical, or expand the designated boundaries compared to the current situation, the current situation in the roads, the distribution of infrastructure resources such as the electricity transmission network, telephone lines, network Drinking water distribution, sewage transmission network and gas distribution network. Despite the complexity of infrastructure distribution, the most important factor that can make the above figure efficient as a decision-making form for local managers is determining the composition of the resident population from the point of view of evacuation. The location of the land in any city and here in the city of Vahdita can hinder disaster control decisions due to its value. For example, the value of commercial properties is sometimes an obstacle of this kind. In the city of Vahdite, the middle position of the stream that passes right

Power System Technology
ISSN:1000-3673
Received: 16-01-2024 Revised: 12-02-2024 Accepted: 07-03-2024

through the center of the city is the cause of this complexity. Generally, the existing uses on the banks of the river are of commercial type, which although it can reduce the loss of life to a great extent for the evacuation reaction, but the financial losses will be more.

2-4- Flood monitoring of the watershed

The main goal of this research is to find the relationship between the upstream area on the amount and shape of the sudden distribution of the flow towards the city of Wahiditeh. In this study, as stated in the previous chapter, first, by using the set of hydrological relationships, the amount of flood and the flow rate were determined according to the morphometric changes of the flood catchment area of Vahadite city. Probable flood hydrograph as a boundary condition in the TUFLOW hydraulic model, which was developed on the urban area using the drone DSM, specifies that from the occurrence of flash floods, damage to a part of the residential fabric can be expected in this section. had a critical condition. The possible return periods for the volume and speed of the flow can lead to the determination of different boundaries of vulnerability inside the city, which the maps of the previous section specify conventionally. In this chapter, the limits of the city's vulnerability have been determined; But in order to determine the importance of the changes in the upstream basin of the city (including canalization and land divisions to changes in the boundaries of the flood basin based on the texture of the land during the past years) in order to prioritize the flood areas in the implementation of the management plans of the most damaged areas, from What is known as the land cover distribution layer, using a dedicated Python script, the regions with the same nature were extracted from the land structure. The method of preparation of the mentioned layer, which was named EO monitoring, has been explained in the previous chapter. Here, this layer (Geology layer) represents the land cover standard in the upstream basin of Vahdati city, which is the criterion for land prioritization studies.

Basically, based on the refined Geology layer as the output of the machine learning method's classifier calculations, flood hazard demarcation is done in the upstream of Vahdatiye city. The approach to evaluate the correctness of this method, which is also the innovative part of the current studies, is by using statistical analysis on a detailed set of Sentinel-2 satellite images and with the criterion of the normalized index of water changes, i.e. NDWI, as described below. It is done.

4-2-1- Geology layer classification model

This composite layer primarily uses 12 bands of short wave infrared (SWIR) to distinguish between different rock types (a band is a region of the electromagnetic spectrum; a satellite sensor can detect the ground in different bands). slow image) and can be prepared by image processing. Each type of rock and mineral reflects short-wave infrared light differently and provides the possibility of drawing a geological map by comparing the reflected SWIR light. Band 8 infrared (NIR) highlights vegetation and band 2 detects moisture, both of which help distinguish terrestrial materials (sentinel-hub, 2021). This composite is useful for locating

Power System Technology
ISSN:1000-3673
Received: 16-01-2024 Revised: 12-02-2024 Accepted: 07-03-2024

geologic structures and features (eg faults, fractures), lithology (eg granite, basalt, etc.) and mining applications; In this research, the variable type of land texture has been considered. Basically, the different textures of the land are used to classify flood-prone areas. Here, by assuming the different effect of the soil texture on the movement of the flood flow, both in the infiltration and the form of the hydrograph of the flow output, first, 7 classes extracted in the mentioned calculations (previous chapter) were determined as demarcation or classification criteria.

Figure (11) shows the Geology layer in the studied area with continuous coloring.

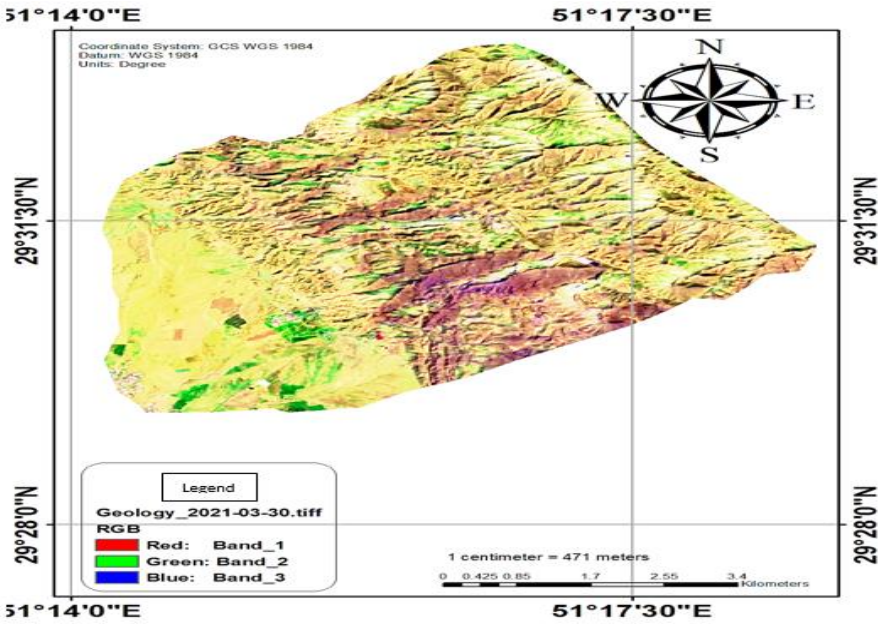

Figure 11 Geology layer of the effective catchment area of the flood of Vahdative city.

Table 2. Changing the initial class of the Geology layer to the final 7 classes.

Old values	New values
0.3975 - 0.595228	1
0.595228 - 0.691846	2
0.691846 - 0.757006	3
0.757006 - 0.810932	4
0.810932 - 0.858117	5
0.858117 - 0.900809	6
0.900809 - 0.970463	7
NoData	NoData

By classifying the Geology layer, the amount of new classes in numbers 1 to 7 was obtained as shown in figures (12) and (13). The limits of changes and the value of each class obtained from the combination of bands mentioned in the extraction and refinement of the machine learning method classifier for the Geology layer are shown in table (1-4).

Power System Technology
ISSN:1000-3673

Received: 16-01-2024 Revised: 12-02-2024 Accepted: 07-03-2024

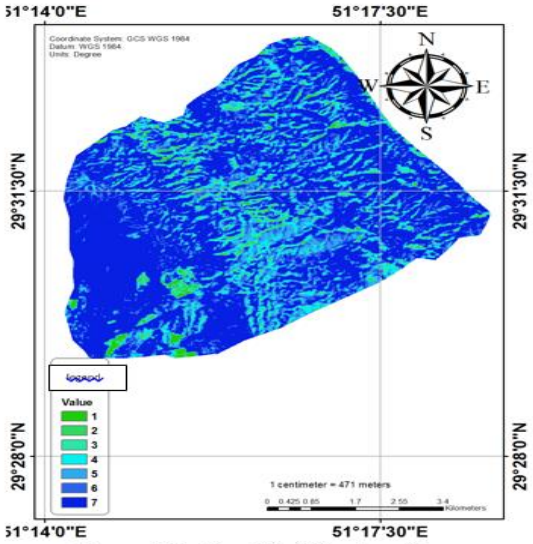

.Figure 13. Classified Geology layer

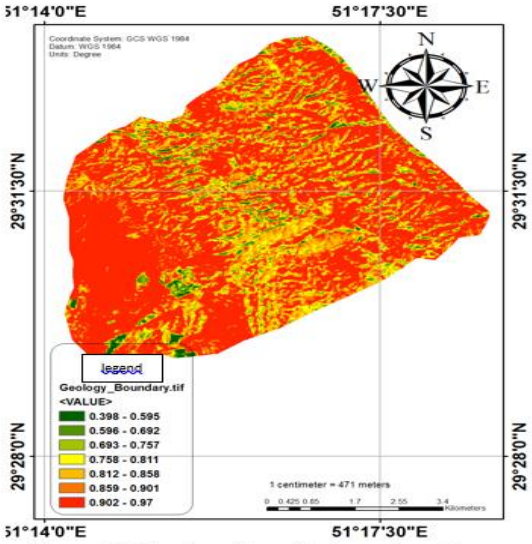

.Figure 12 Geology layer before class change

In figures (14) to (21), you can see the location limits of spatial layers of classes 1 to 7 on the NDWI index layer. The NDWI index itself was calculated as described in the previous chapter from the analysis of bands of Sentinel-2 satellite images. The boundaries show that the distribution of each class is not necessarily limited to one altitude or geographical direction. However, the density of class 1 is very small compared to class 7.

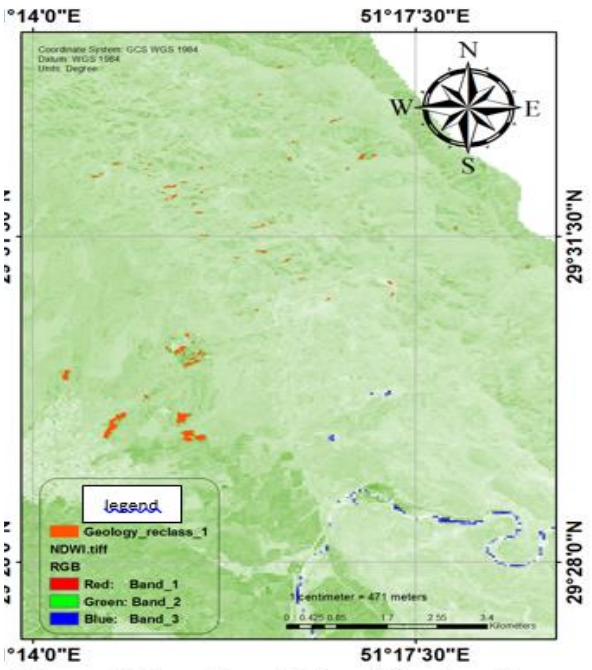

.Figure 15 Location of class 1 Geology layer

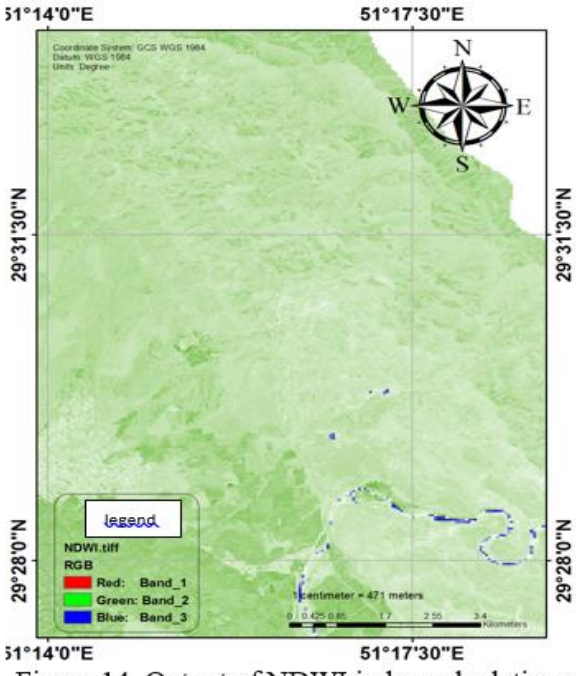

.Figure 14. Output of NDWI index calculations

Power System Technology
ISSN:1000-3673

Received: 16-01-2024 Revised: 12-02-2024 Accepted: 07-03-2024

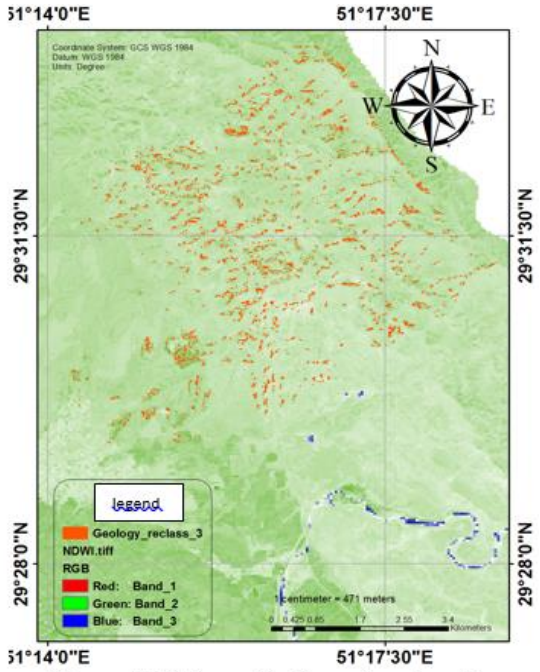

.Figure 17. 3 layer Geology class location

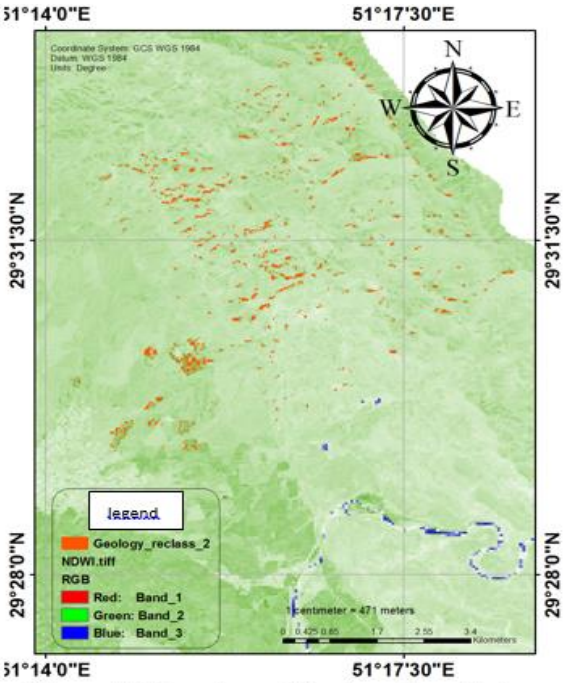

.Figure 16. Location of Geology layer 2 class

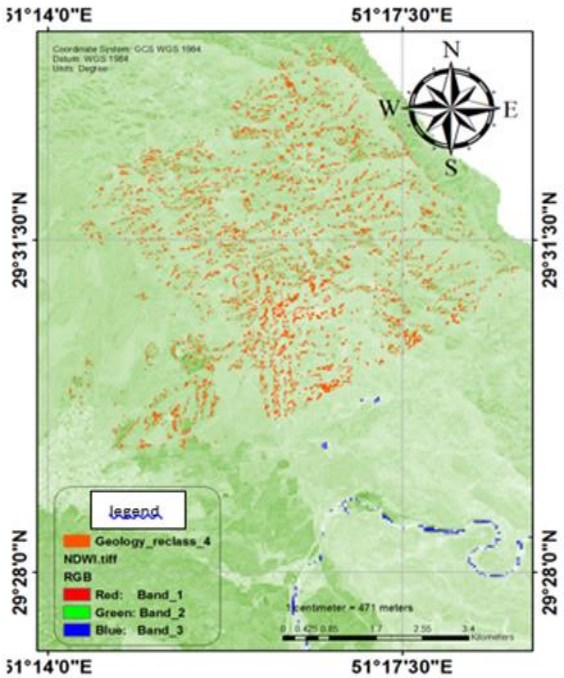

Figure 18. Location of the 4-layer Geology .class

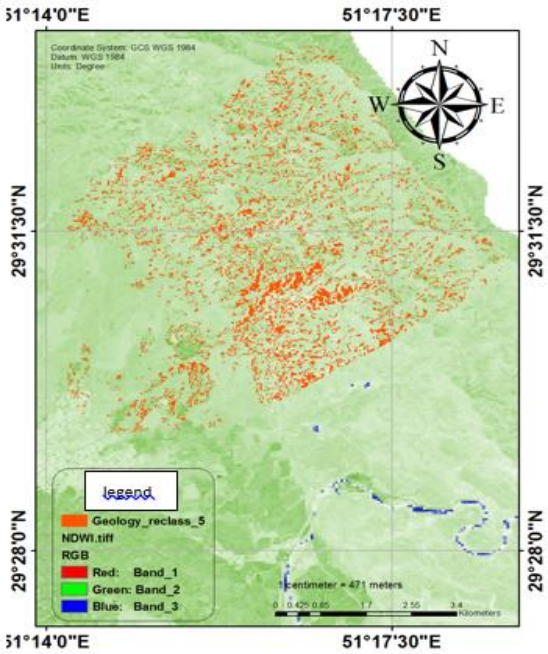

.Figure 19. 5 layer Geology class location

Power System Technology
ISSN:1000-3673

Received: 16-01-2024 Revised: 12-02-2024 Accepted: 07-03-2024

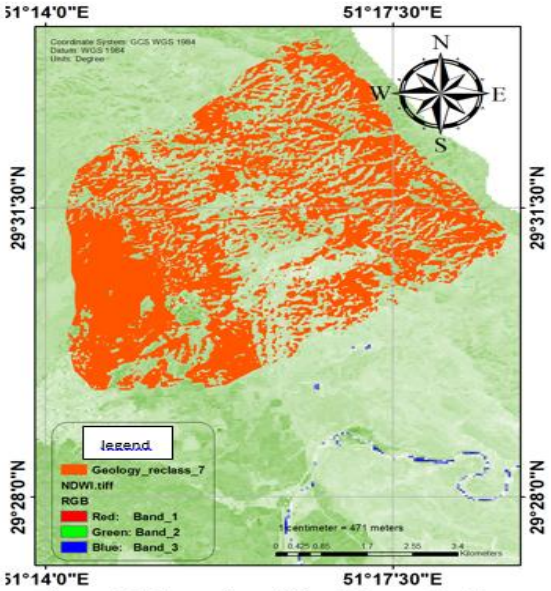

Figure 21. Location of the 7-layer Geology .class

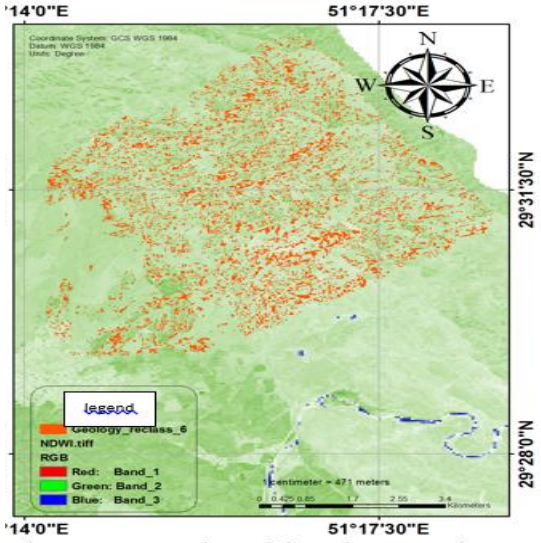

Figure 20. Location of the 6-layer Geology .class

Also, in the general flood area of Vahdatieh city, the value of NDWI and Moisture Index has been calculated during the 5-year period from 2016 to 2021. NDWI index has been chosen here to track the effect of flood rains on the studied area. This amount has also been calculated on the entire catchment area of the second level of Madar. Pictures (22) and (23) show the values of NDWI and Moisture Index for the entire catchment area of the study area in the last period.

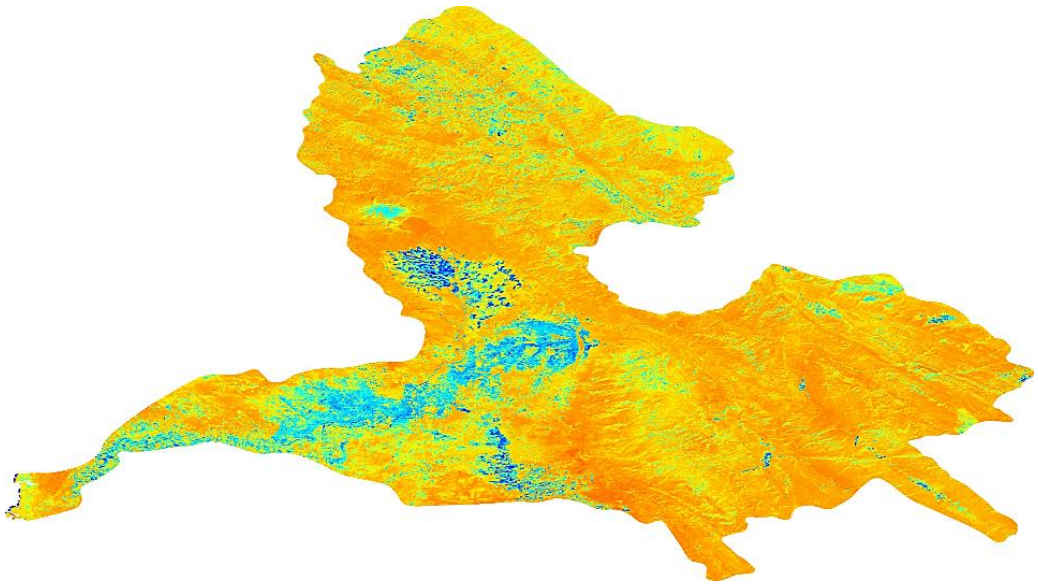

Figure 22 Calculation of the Moisture Index in the main catchment area of the study area.

Power System Technology
ISSN:1000-3673
Received: 16-01-2024 Revised: 12-02-2024 Accepted: 07-03-2024

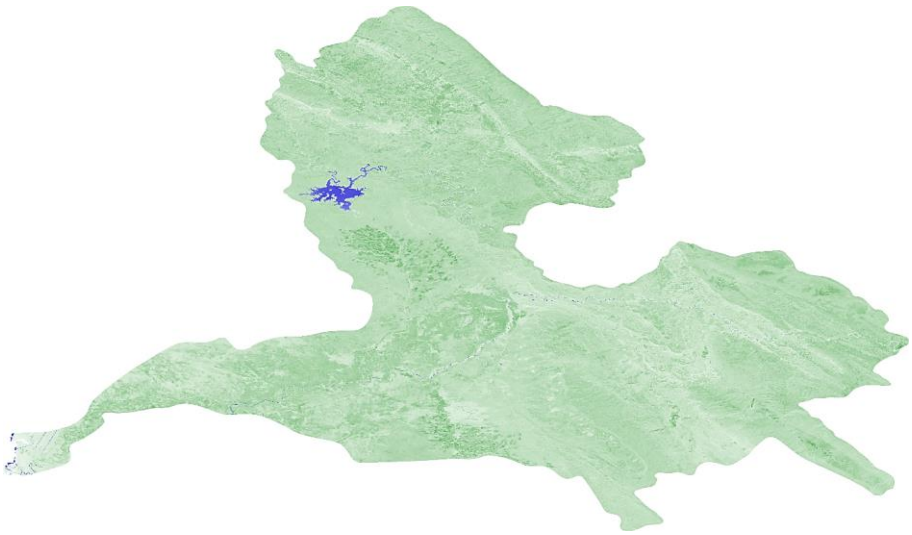

Figure 23 Calculation of the NDWI index in the main catchment area of the study area.

The result of these calculations, which is the result of processing dozens of images from the Sentinel-2 satellite, is shown in the diagram of Figures (24) and (27) in the form of diagrams with limits of reliability changes. It should be noted that the Moisture Index, which behaves opposite to NDWI, can be checked as an evaluator of the correctness of the method of calculating each case of NDWI extraction.

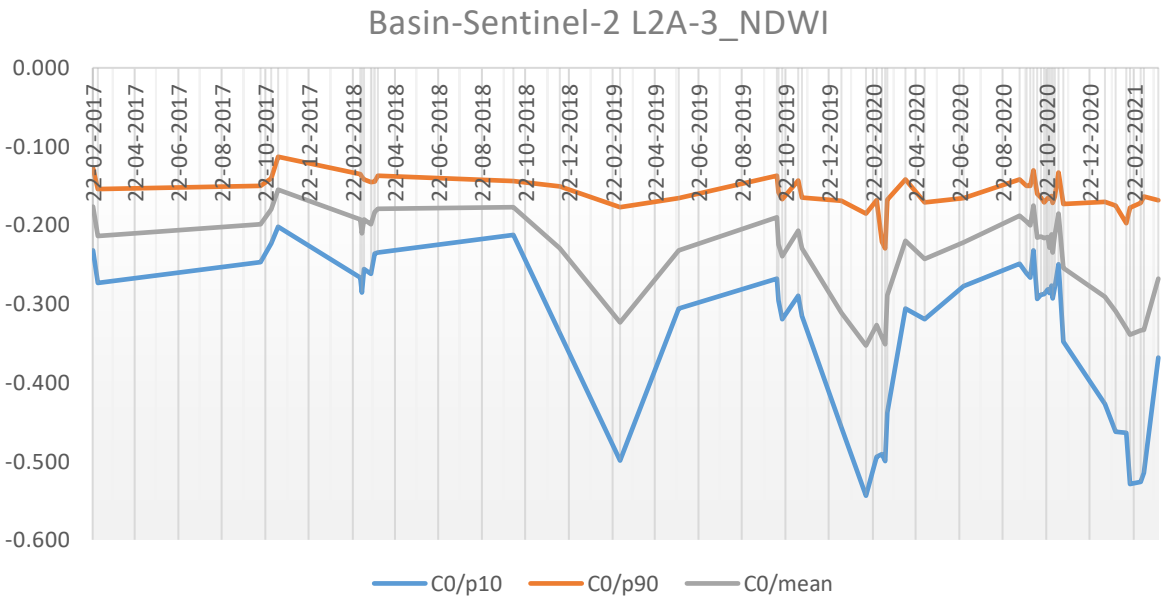

Figure 24. NDWI index and about 5-year changes in the main catchment area of the study area.

Power System Technology
ISSN:1000-3673
Received: 16-01-2024 Revised: 12-02-2024 Accepted: 07-03-2024

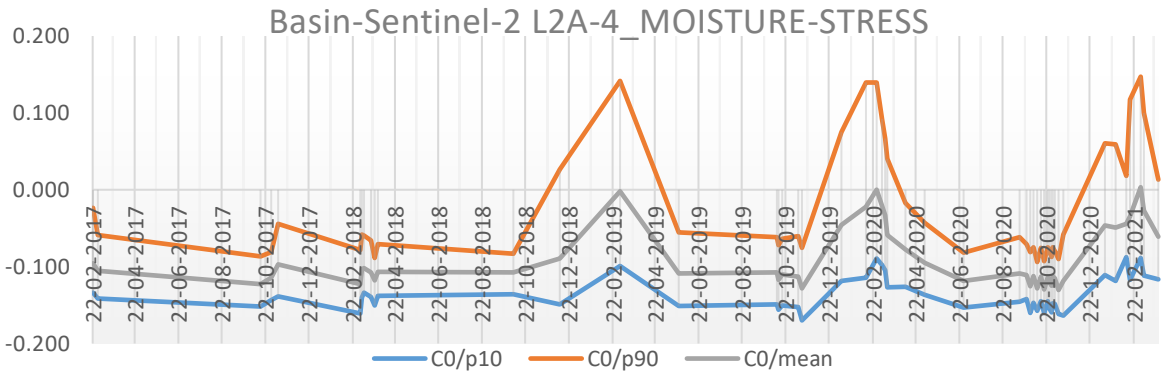

Figure 25. MOISTURE-STRESS index and about 5-year changes in the mother catchment area.

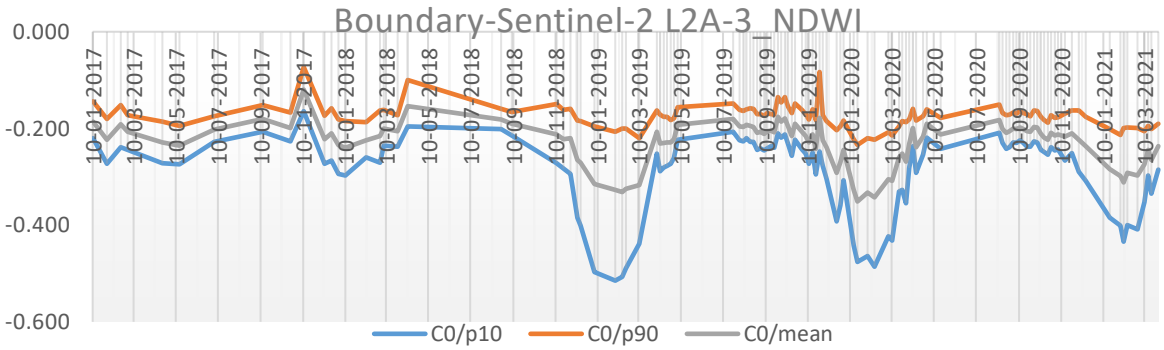

Figure 26. NDWI index and about 5-year changes in the effective flood basin of Vahdatiye city.

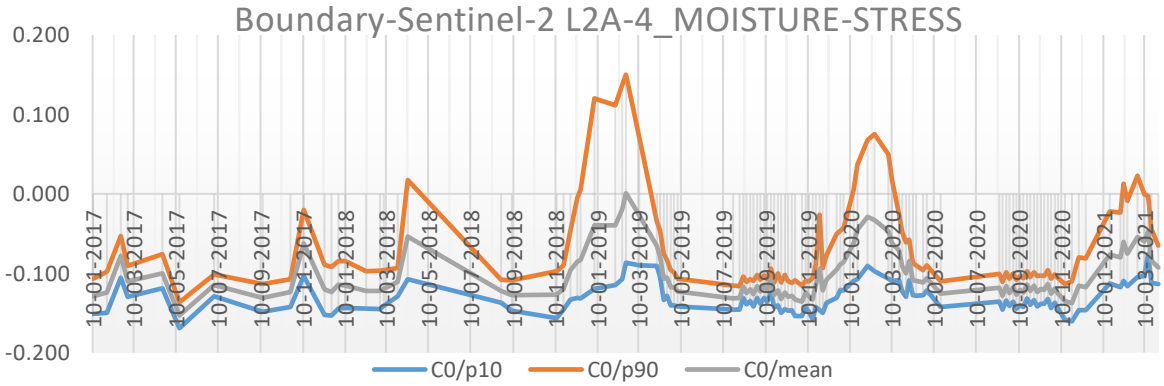

Figure 27. MOISTURE-STRESS index and about 5-year changes in the area of the effective flood basin of Vahdatieh.

Power System Technology
ISSN:1000-3673
Received: 16-01-2024 Revised: 12-02-2024 Accepted: 07-03-2024

Figures (28) and (29) as a combination of the above indices, show the value of each item in a comparative manner without the threshold of reliability changes and only as an average value. The numerical changes of average NDWI clearly show that in the studied area, there is no specific blue zone that returns the index figure in a positive way. Also, the returned figure in the whole period indicates the lack of dense vegetation. This index mainly reflects dry plants and soil in both cases. The changes in the index value are related to the seasonal changes of the separated water areas and vegetation due to the growth in the conditions of floods.

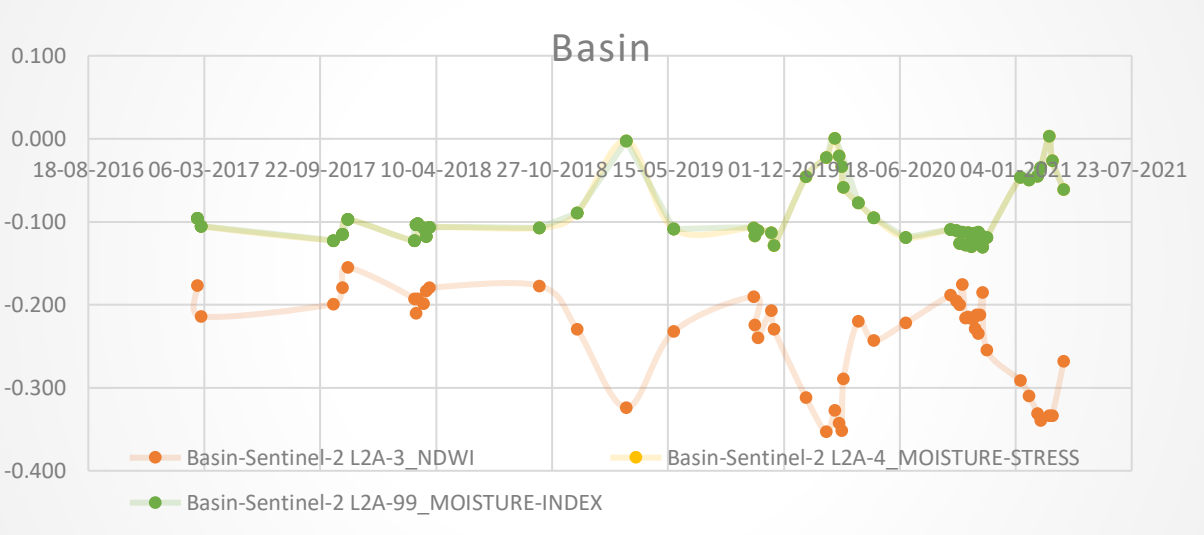

Figure 28. Comparison of MOISTURE-STRESS and NDWI indices in the Mader catchment area.

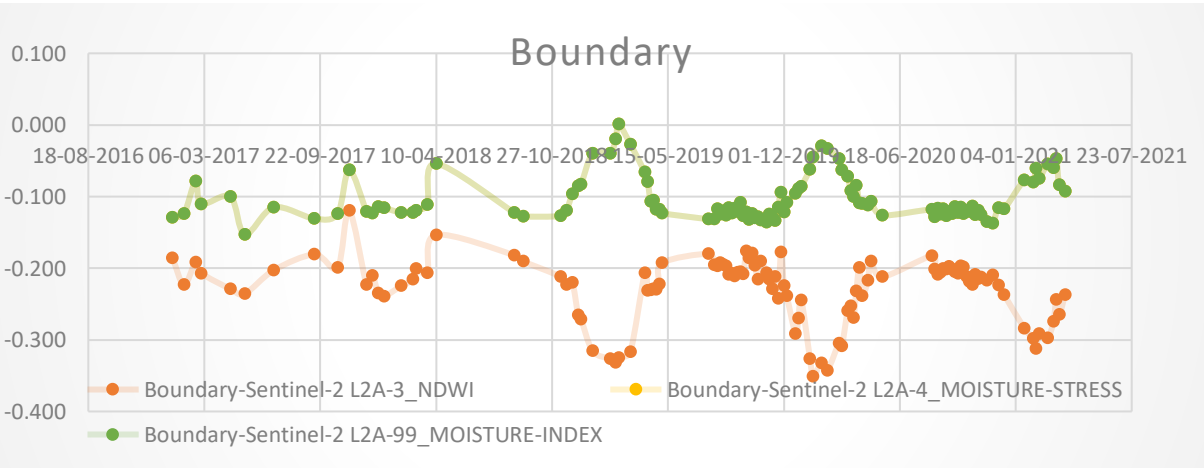

Figure 29. Comparison of MOISTURE-STRESS and NDWI indices in the area of the effective flood basin.

Power System Technology
ISSN:1000-3673
Received: 16-01-2024 Revised: 12-02-2024 Accepted: 07-03-2024

For 7 divided classes of Geology layer, the NDWI change index value was calculated based on dozens of Sentinel-2 satellite images. The result similar to what was obtained in the previous step is drawn in figure (30). It can be clearly seen that the behavior of each diagram follows the general diagram of the flood prone area. At the same time, the behavior of the general changes of the NDWI diagram in the flood-prone area upstream of Vahdatiye city is consistent with the behavior of the second-order watershed.

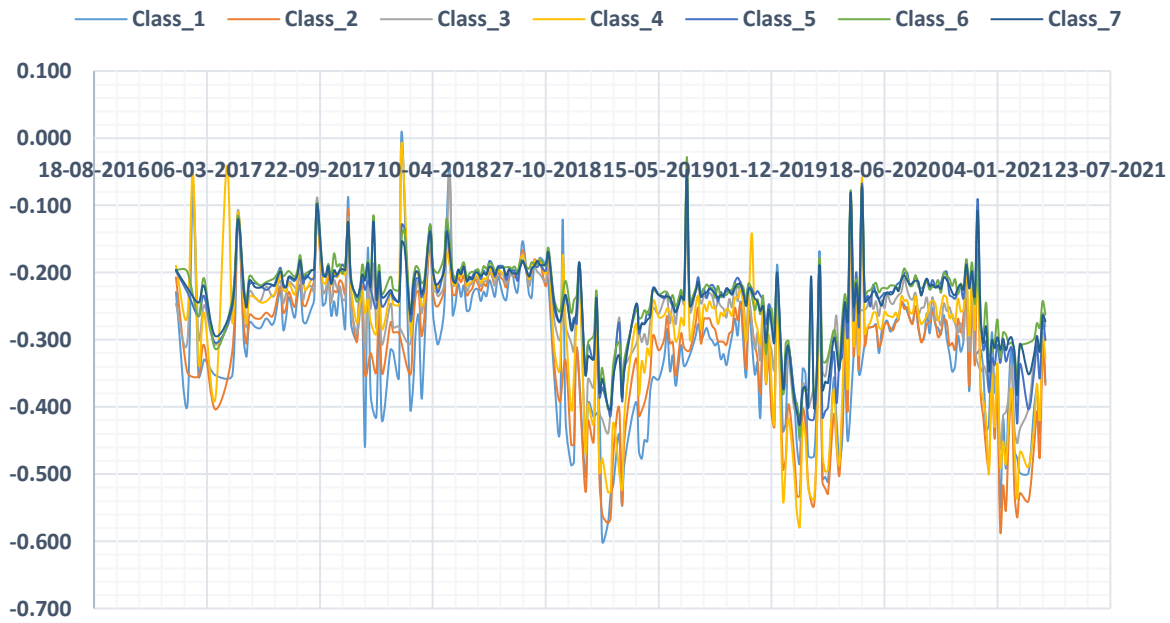

Figure 30. Changes in the NDWI index in the 5-year period of 7 Geology classes of the effective flood catchment area of Vahdatiye city.

The numerical value of the above graph is given in table (2) as a statistical summary. The fitted linear slope in each case represents the simplified form of change over the five-year period. The minimum and maximum figures of the index along with its average value are given in three columns. It can be seen that the minimum average value occurred in classes 1 to 4 and the maximum value of the average index occurred in classes 5 to 7. Class 7, for example, here shows the sections that are related to the vegetation and agricultural land. Therefore, the growth of vegetation in periods of the year that lead to an increase in the value of the NDWI index has been predictable.

Power System Technology
ISSN:1000-3673
Received: 16-01-2024 Revised: 12-02-2024 Accepted: 07-03-2024

Table 3. Statistical summary of the NDWI index in the 5-year period of 7 Geology classes in the effective flood basin of Vahdatiye city.

Title	Linear regression slope	NDWI index			
		minimum	maximum	average	Changes
Class 1	-0.0000808	-0.599	0.010	-0.313	0.609
Class 2	-0.0001026	-0.584	-0.066	-0.310	0.518
Class 3	-0.0000714	-0.462	-0.048	-0.264	0.414
Class 4	-0.0001129	-0.577	-0.007	-0.280	0.571
Class 5	-0.0000597	-0.425	-0.067	-0.244	0.358
Class 6	-0.0000575	-0.445	-0.028	-0.233	0.418
Class 7	-0.0000574	-0.426	-0.047	-0.240	0.379

In addition, it is shown in table (3) that each determined class has an average height of the topography of the earth's surface. This table is based on zonal analysis on the DEM layer received with an accuracy of 30 meters on the studied area in the GIS environment. The classes that represented the highest value of the average index are located at a lower altitude. This issue confirms the content of the last paragraph, which considered the areas with vegetation and post-agriculture related to the increase in the value of the index.

Table 4. Spatial analysis of DEM layer in about 7 Geology classes.

code	Number of cells	area (square meter)	minimum	maximum	average	standard deviation	Total
1	305	253884.926	93	940	206.7639344	170.560	63063
2	1089	906494.050	94	939	356.5151515	211.334	388245
3	2077	1728914.732	96	940	361.2272508	193.780	750269
4	3484	2900115.034	90	938	332.0852468	180.188	1156985
5	5119	4261104.723	90	928	321.4315296	169.752	1645408
6	6153	5121816.246	90	935	321.5988948	176.969	1978798
7	24319	20243368.970	87	930	311.0497553	208.855	7564419

The effect of land geology on floods with a focus on special soil maintenance

In this study, we have investigated the question of whether the changes in flood volume in an alluvial catchment basin can be caused by increasing the flow level and water depth in the river network of that basin, and changing the shape of the waterway network (in Other geological

Power System Technology
ISSN:1000-3673
Received: 16-01-2024 Revised: 12-02-2024 Accepted: 07-03-2024

uses prone to flow release), compensate for a part of the reduction of aquifer nutrition following the development of impervious surfaces? Because this can affect the magnitude of urban floods and the risk of flooding, and in determining indicators such as FRI which was calculated in the previous section. A basic assumption in the development of underground water flow models is that increasing the water level in the water channel elements, as long as the water level in the aquifer is lower than the river bed level, has no effect on the amount of infiltration from the river into the aquifer. . The requirement to determine the aquifer feeder network, which is also considered the equivalent of the main flood flow loss network, in this case assuming the homogeneity of the catchment basins in the distribution of flood flow despite the changes in their permeable levels, can lead to deviations in the estimation. soil retention capacity (Sb) in the watershed. Because the hydrograph of the artificial SCS unit, in determining the volume of flow, is dependent on the accuracy of the previous soil moisture capacity relationship and the effective precipitation conversion equations in the study area, and in determining the flood propagation method, it is dependent on the parameters of the runoff hydrograph equation; This second parameter itself is affected by the morphological conditions of the catchment area, or in other words, the condition of soil storage capacity (assuming the presence of cesspools and infiltration rate, etc.). The value assumed as an average in normal conditions without considering a probability distribution function.

By determining the location of the waterway network in two extreme flood conditions, we investigated the problem mentioned in the previous paragraph. In order to solve the problem of separation of watershed flow elements, the 3D finite difference model was implemented, calibrated and verified in GMS software in a period of 38 months with MODFLOW 2005 mathematical code. The developed model includes 22 vertical layers with a variety of soil parameters based on drilling boreholes, and more than 3.5 million cells in dimensions of 10 meters by 10 meters. The development of the model was carried out in five steps: implementation of the stable model, recalibration of the stable model, implementation of the unstable model, recalibration of the unstable model and validation. The results show that of the 694.5026826 cubic meters of water entered into the aquifer during the period of 76 months (including the forecast period), the share of direct feeding was 10%, permeable boundaries were 81% and the waterway network was 9%. Of this amount, the reserve figure in the area is only 15374.458 cubic meters. Also, of the amount of 807.5026863 cubic meters of water removed from the aquifer in the two-year period, the share of nutrition (evaporation) was about 10%, permeable borders 87% and waterway network 0%. In addition, the share of exploitation wells has been 3%, which has led to a local drop around their coordinates. Also, the output storage flow during this period was 439.4035 cubic meters. The direction of the flow is from the northeast to the southwest, in line with the natural slope of the area. The highest flow speed occurs in the border areas of GHB and the highest water level rise and fall occurs in steep areas. The prepared model shows that the aquifer has a limited capacity in water accumulation, that with every feeding by precipitation, a major part of the incoming flow to the area is transferred to the area as a drain through the waterway network and permeable boundaries. be made The

Power System Technology
ISSN:1000-3673
Received: 16-01-2024 Revised: 12-02-2024 Accepted: 07-03-2024

criteria for the changes in nutrition of the areas have been different nutrition coefficients. The results in this section specify the different speed of flow entry and exit from the model elements. In this way, it can be expected that with the development of urban use, especially with the change of the route of the waterway network or the speed of flow penetration, the amount of aquifer recharge will decrease significantly. In the prediction model, it can be expected that there will be a difference and a 19.119 percent reduction in nutrition due to urban development in the area of 2 regions. This output is extracted based on the results of balance calculations of the simulation model.

In the diagram of Figure (44), which represents the elements of the balance in the entire aquifer, the dotted red line represents the amount of drained water (almost zero) and the dashed blue line represents the amount of water infiltrated from the river network. The yellow bar graph is the average discharges of the total storage in monthly intervals for the study area. These three values should not be directly compared to each other. Because the MODFLOW model does not specify the discharge figures for the River package. Rather, only based on the infiltration and drainage output of the river in the model balance, it is possible to understand the origin of the discharge observed in the study area. In addition, a certain part of observed discharge is the result of direct transfer of surface water in the aquifer to the river network after rainfall. The trend similar to the black diagram as water exiting the permeable boundary of the aquifer indicates that a part of the water entered through the exchange zone leaves the aquifer.

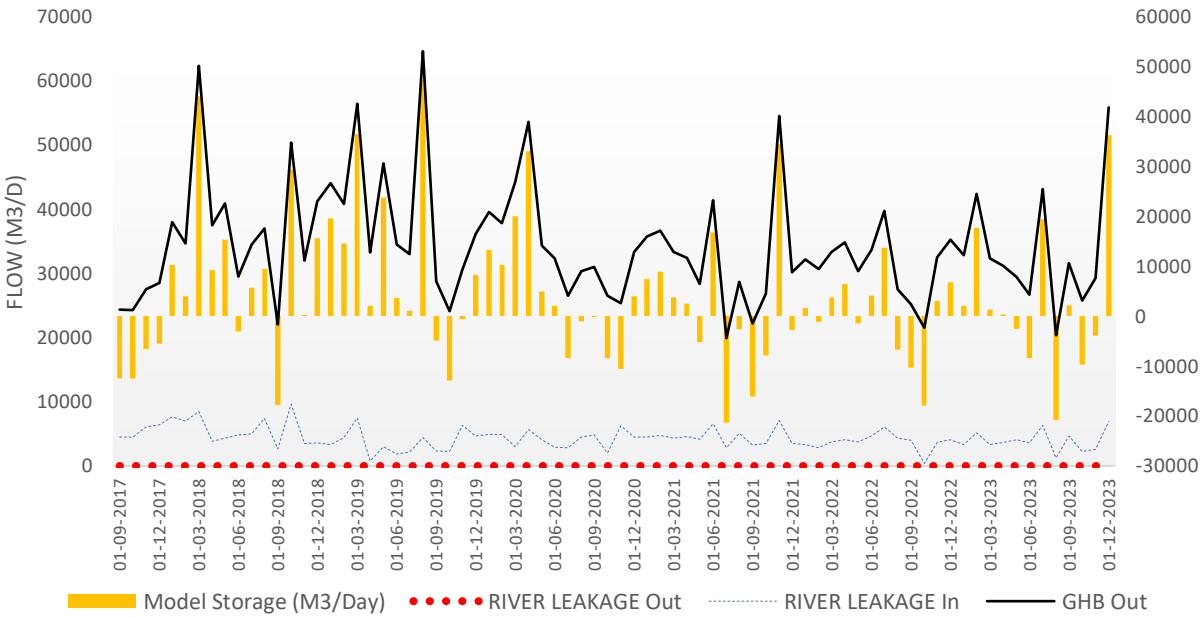

Figure 44. Comparison of infiltration from the waterway network of the model and the discharge of the waterways reported by Bilan.

Power System Technology
ISSN:1000-3673
Received: 16-01-2024 Revised: 12-02-2024 Accepted: 07-03-2024

In the next step, based on the approach of assigning the cellular nature of the finite difference network of the MODFLOW model, by determining the range involved in the feeding of this area in the surface flood model based on the soil texture and the target area, the flow loss and runoff penetration into the soil was determined.

The amount of water that can be stored in the soil, under the name of storage capacity of the basin (Sb), depends on the type and texture of the soil and generally follows the pattern in the figure (45-4). Also, the measurements made to estimate the VWC of this area (using the global FLDAS model) are shown in the diagram of the present figure with daily time intervals. Our idea is to create a continuous layer of this coefficient, which is practically impossible to calculate throughout the basin even with the addition of observation sensors. From the combination of the standardized layers, the depth of the two-dimensional flood flow with the standardized layer of impermeability of the surfaces. In such a way that the maximum value of the basin capacity at the place of VWC estimation in the downstream of the urban basin (outflow point) with a value of 40% and due to the presence of areas with permeability close to zero in this range, the pattern in figure (45) which It shows the minimum value in the soil of about 13%, with a figure of 1% was used to standardize the layers.

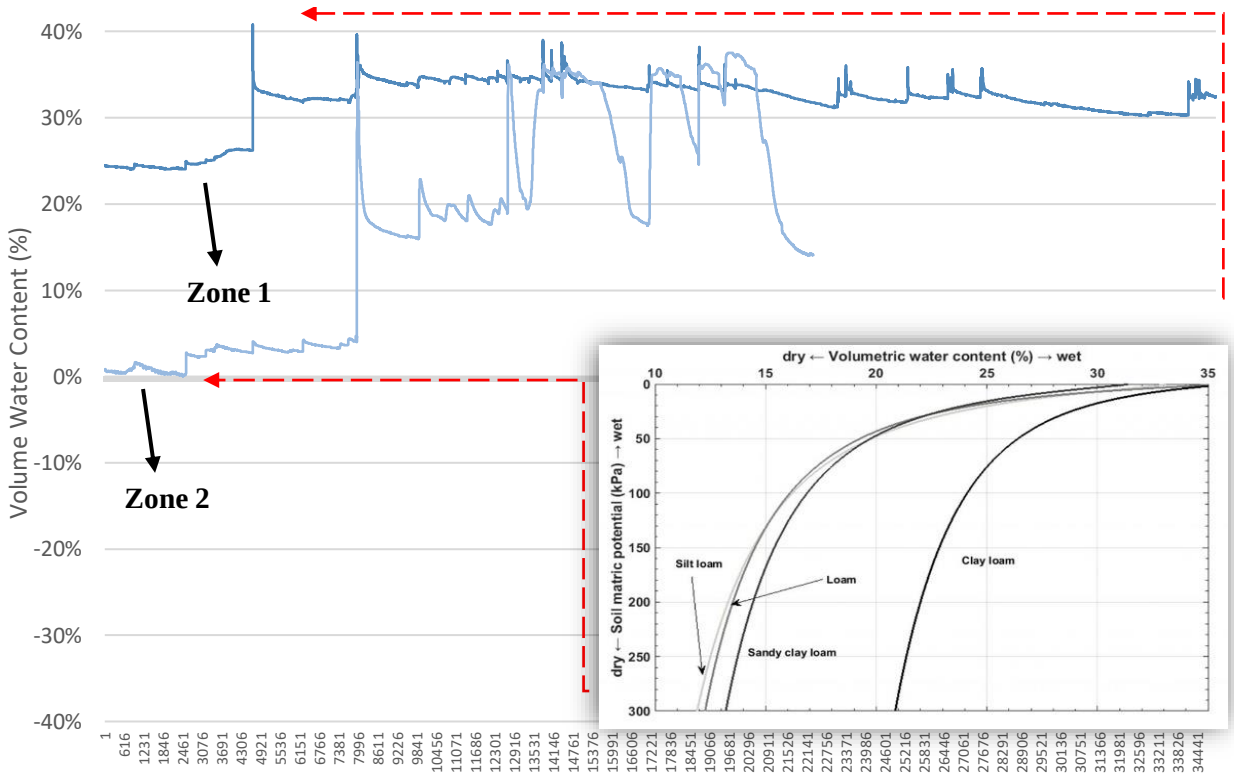

Figure 45. The basic pattern of distribution of soil saturation percentage in the study area and VWC observation figures of the FLDAS model.

Power System Technology
ISSN:1000-3673

Received: 16-01-2024 Revised: 12-02-2024 Accepted: 07-03-2024

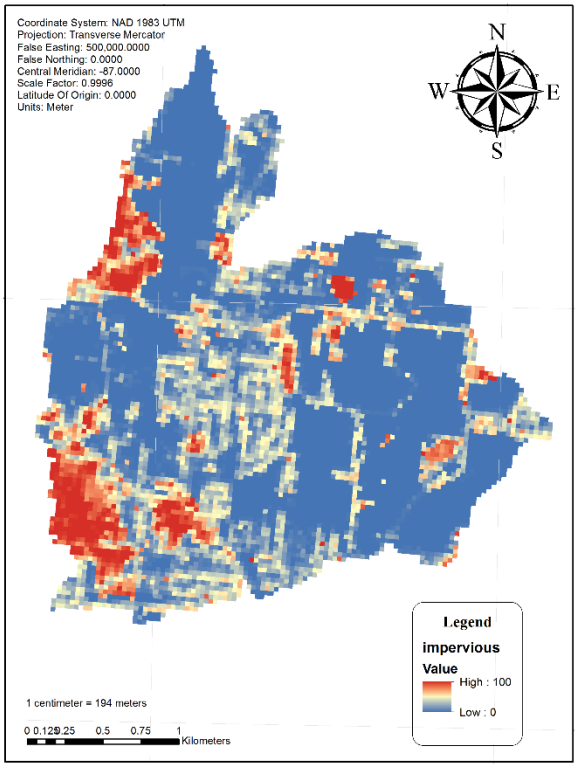

Figure 47. Impermeable layer (IS) in the .study area

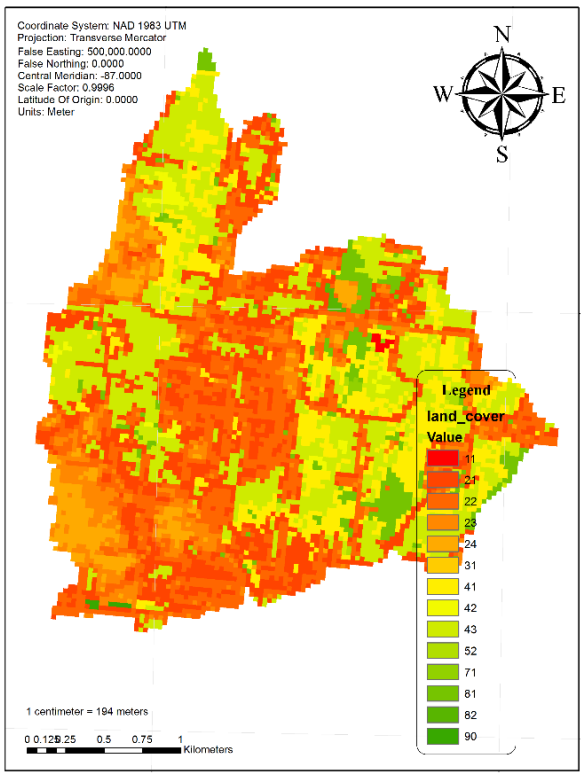

Figure 46. Diversity of land cover layer in .the study area

The two-dimensional flood reference layer is the output of the TUFLOW hydraulic model for a historical rainfall with a return period of 100 years with a total volume of 242.187 mm in 24 hours. The rainfall distribution pattern was prepared based on the third type of SCS hytograph. The computational base hydrograph of the area was also prepared using the SCS method, and the amount of rainfall duration equal to 20 minutes was suggested by this hydrograph. Therefore, by preparing the precipitation volume of 57.622 mm, the hydraulic model was implemented in the Aquaveo SMS software environment (Figure 48).

The results of the implementation of the hydraulic model in the initial step indicated a good match of the maximum flow rate and the relative difference in the amount of volume and the time of the peak flood event. This difference can be considered due to the weakness of flood trending in the hydraulic method and also the difference between the loss calculation methods in the SCS-CN hydrological approach and the two-dimensional TUFLOW flood hydraulic equations which were introduced to the model with the Initial Losses-Continues Losses method. . Table (4-7) shows the percentage of each user class and its equivalent coefficients for the infiltration parameter using the ILCL method used in the flood model.

Power System Technology
ISSN:1000-3673
Received: 16-01-2024 Revised: 12-02-2024 Accepted: 07-03-2024

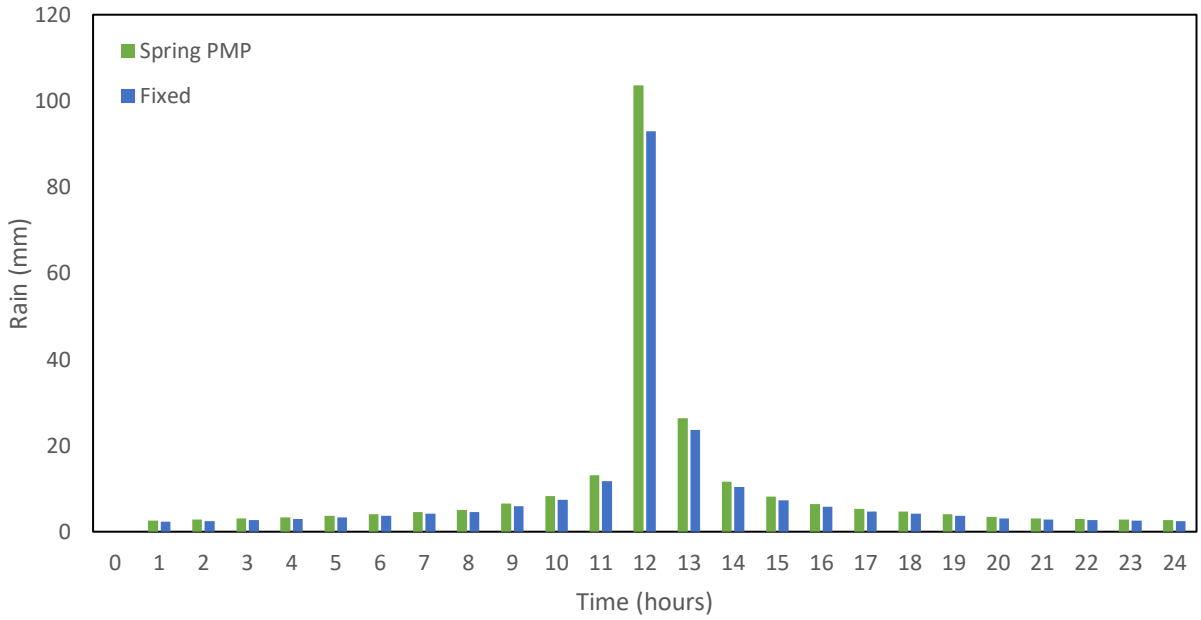

Figure 48. SCS Type III hytograph of precipitation and amount separation in the proposed period of SCS-CN dimensionless hydrograph.

Table 7. The loss ratio of the Initial Losses-Continues Losses method based on the IS coefficients in the unity range.

IS	TUFLOW Run-1			TUFLOW Run-2			Land Cover Name
	IL (mm)	CL in Base time	CL (mm/hr)	IL (mm)	CL in Base time	CL (mm/hr)	
0.000%	0.76	34.19	180.40	15.46	30.76	162.33	Open Water
8.405%	0.70	31.32	165.24	14.16	28.18	148.68	Developed, Open Space
33.199 %	0.51	22.84	120.51	10.33	20.55	108.44	Developed, Low Intensity
61.290 %	0.29	13.23	69.83	5.98	11.91	62.84	Developed, Medium Intensity
86.235 %	0.10	4.71	24.83	2.13	4.23	22.34	Developed High Intensity
0.000%	0.76	34.19	180.40	15.46	30.76	162.33	Barren Land (Rock/Sand/Clay)

Power System Technology
ISSN:1000-3673
Received: 16-01-2024 Revised: 12-02-2024 Accepted: 07-03-2024

0.000%	0.76	34.19	180.40	15.46	30.76	162.33	Deciduous Forest
0.000%	0.76	34.19	180.40	15.46	30.76	162.33	Evergreen Forest
0.000%	0.76	34.19	180.40	15.46	30.76	162.33	Mixed Forest
0.000%	0.76	34.19	180.40	15.46	30.76	162.33	Shrub/Scrub
0.000%	0.76	34.19	180.40	15.46	30.76	162.33	Grassland/Herbaceous
0.000%	0.76	34.19	180.40	15.46	30.76	162.33	Pasture/Hay
0.000%	0.76	34.19	180.40	15.46	30.76	162.33	Cultivated Crops
0.000%	0.76	34.19	180.40	15.46	30.76	162.33	Woody Wetlands

The average value of the flow depth layer with cell dimensions of 10 meters by 10 meters in the form of a raster from the initial interval of the historical event of 100 years of rainfall to the peak moment of the flood at the outlet point of the basin, in a total of 13 time steps of 6 minutes, the weight of the coefficient of this parameter in determining The distribution moisture of the soil was determined in this research. In this way, in the areas with the maximum depth of the flow, the maximum saturated moisture and in the areas with the minimum depth, the minimum weight of the saturated moisture was assigned through a linear regression equation (Figure 49).

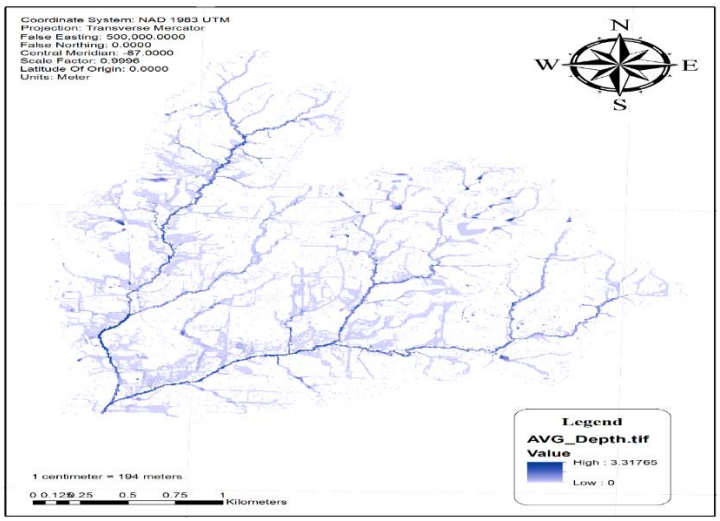

Power System Technology
ISSN:1000-3673

Received: 16-01-2024 Revised: 12-02-2024 Accepted: 07-03-2024

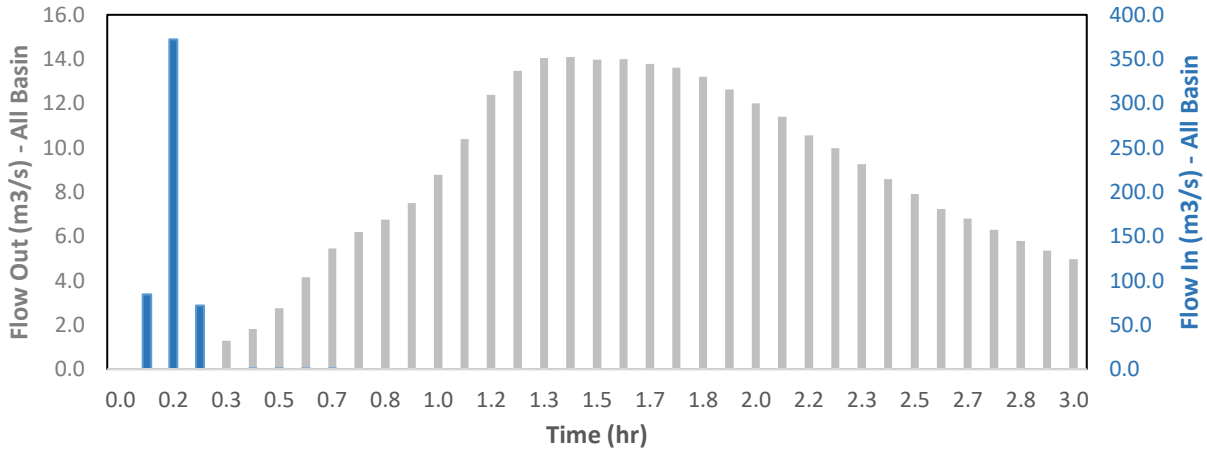

Figure 49. Flood distribution and hydrograph in the initial implementation of the hydraulic model.

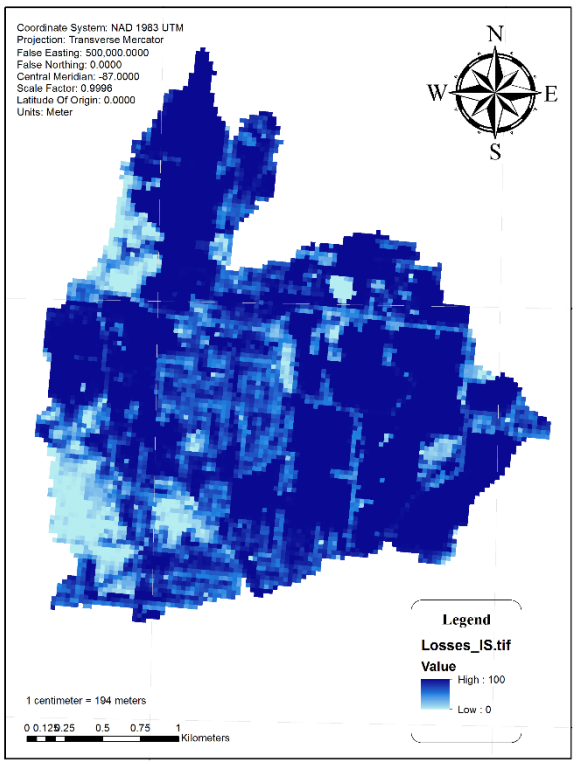

Figure 51. Standard coefficient of .impermeability distribution

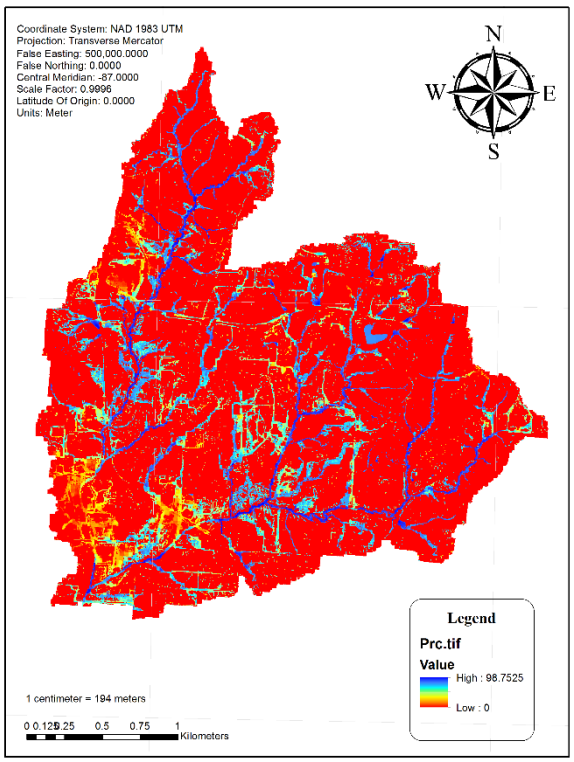

Figure 50. Depth distribution coefficient of .flood flow

Power System Technology
ISSN:1000-3673

Received: 16-01-2024 Revised: 12-02-2024 Accepted: 07-03-2024

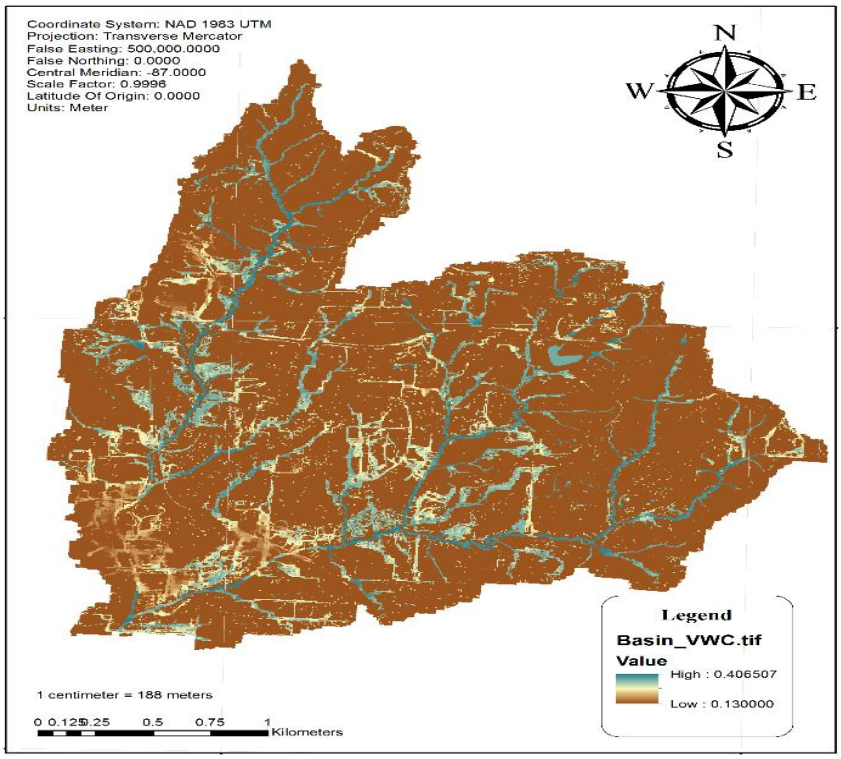

Figure 52. The distributed coefficient of the soil holding capacity parameter (Sb) in the city of Wahiditeh.

Figures (50) and (51) show the depth-base coefficients as the output of the initial TUFLOW model and infiltration-base, which are the basis for determining the distribution of water storage capacity in the basin. The initial implementation of the TUFLOW model was prepared based on the effective flood value of the SCS-CN equations (Figure 52). Also, figure (52) is the result of the spatial combination of the mentioned coefficients in the environment of the geographic information system. The maximum value in this form is equal to about 40% in the grid cells of the south of the aquifer at the outlet and the minimum value is about 1% in areas with low permeability or flood depth close to zero. The simulation output is shown in figure (55) for the time intervals of the event.

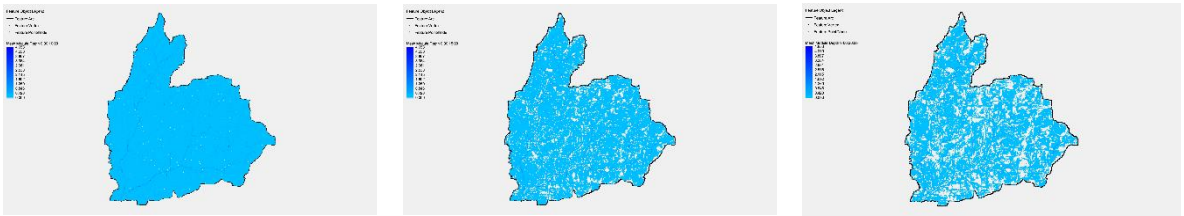

Power System Technology
ISSN:1000-3673

Received: 16-01-2024 Revised: 12-02-2024 Accepted: 07-03-2024

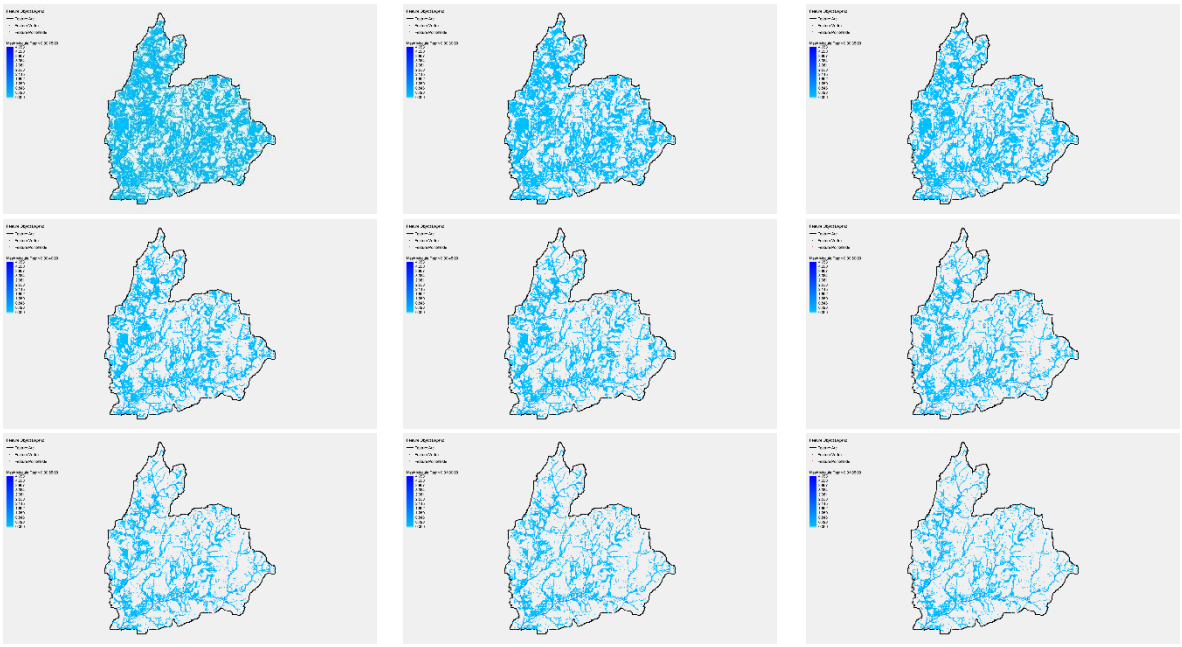

Figure 53. Two-dimensional distribution of floods after deduction of rainfall losses by ILCL method until the moment of peak outflow from the area.

The second stage of hydraulic calculations uses the studies of Wang (2018) in order to determine the volume of the current flood in the area, which ultimately leads to the production of a new depth layer of runoff. This equation defines the soil storage capacity layer distribution based on the probability distribution assumption. Therefore, in general, in extreme conditions (historical floods), the amount of runoff volume is closer to the reality and larger than the initial equations of SCS-CN. The magnitude of the calculated value at a reasonable threshold can challenge the water holding capacity in the basin by preparing the standardized layers again. Therefore, by obtaining a probabilistic value of the parameter of figure (a) in the SCS-CN base distribution equation of Wang (2018), by calculating the value of the moisture ratio as an indicator of water storage in the soil, in two ways, one based on the model results and One was derived from the new theory of SCS-CN, which is based on the point probability distribution function at the watershed scale, and the other was prepared based on the results of the general SCS-CN model. However, in order to calculate the new SCS-CN equations, there is a need to estimate probabilities of the basin shape parameter. In this way we will have:

$$\frac{W}{P} = \frac{1 + \frac{\sqrt{(m+1)^2 - 2am}}{1-\psi}\Phi_{sc\,(Model)} - \sqrt{(1 + \frac{m+1}{1-\psi}\Phi_{sc\,(Model)})^2 - 2am(\frac{\Phi_{sc\,(Model)}}{1-\psi})}}{a} \quad (1)$$

Power System Technology
ISSN:1000-3673
Received: 16-01-2024 Revised: 12-02-2024 Accepted: 07-03-2024

where the parameter m is calculated based on two variables a and ψ. The variable a will be between two numbers 0 to 2 (Wang, 2018). This parameter was calculated as β between 0.01 and 5 in the studies of Wood et al. (1992); which determines the convexity and concavity of the soil storage capacity distribution curve. If the sensitivity value of the graph mentioned between the two indicators is determined, it can lead to the refinement of parameter a as the shape parameter in the new SCS-CN equation.

$$Q = \frac{(a-1)P - S_p\sqrt{(m+1)^2 - 2am} + \sqrt{[P+(m+1)S_b]^2 - 2amS_b^2 - 2aS_bP}}{a} \quad (2)$$

The following equation shows surface runoff as a function of precipitation (P), average water storage capacity in the basin soil (Sb), storage capacity distribution shape parameter (a) and initial soil moisture (ψ). In this equation, the estimation of the parameter a is practically the same as the parameter Cp of the unit hydrograph and requires trial and error based on observational data. However, here, assuming the equalization of the discharge obtained from the new method of determining the flood runoff, with the output of the unit hydrograph calculations determined based on the initial form of the SCS-CN method (Section 2), an initial approximation of it was assumed.

$$\phi_{sc\,(Model)} = \frac{S_b - S_0}{P} = \frac{S_p}{P} \quad (3)$$

The variable $\phi_{sc\,(Model)}$ in equation (5) was calculated based on the output of the recalibrated model of the area (infiltration rate, precipitation and average storage capacity of the basin) for all time intervals. Figure (54-4) shows the distribution of two soil storage indices ϕ_{sc} and moisture ratio $\frac{W}{P}$ for the two mentioned methods in the range of 0 to 300 horizontal units.

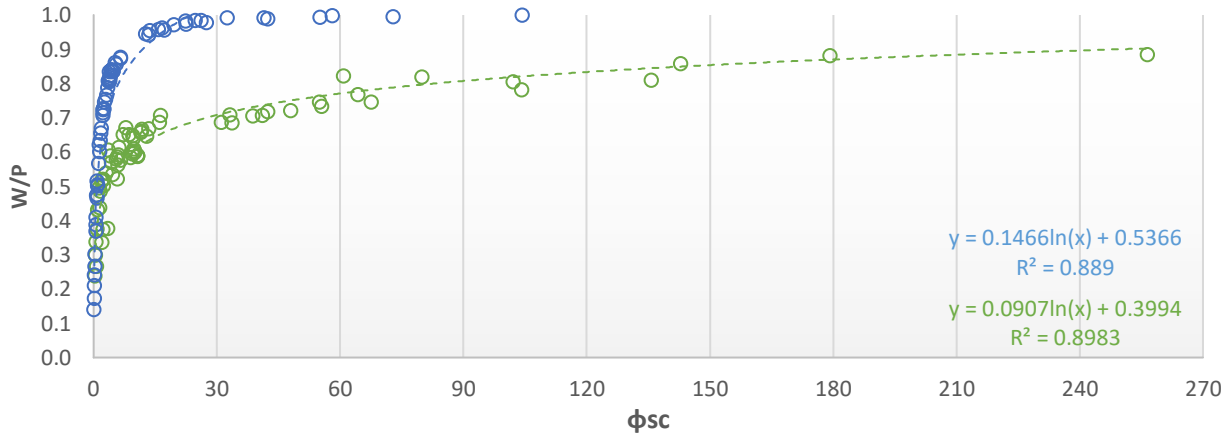

Figure 54. Distribution of soil storage capacity index ϕ_{sc} versus soil moisture ratio $\frac{W}{P}$ from theoretical model and VWC of FLDAS model.

Power System Technology
ISSN:1000-3673
Received: 16-01-2024 Revised: 12-02-2024 Accepted: 07-03-2024

- Reliability analysis of the nature of flood propagation

To determine the threshold of changes in the parameters of figure a in the method of determining the runoff volume of the hydrograph unit of the new SCS-CN equations, it was done by determining the reliability threshold in a performance function of the magnitude of the event. Reliability is defined as the importance function g(X) being positive; in such a way that P {g(X)>0}. In other words, reliability is the probability that the random variable X=(X1, X2..., Xn) is located in the safe region g(X)>0. And in this way, the probability of failure is defined as g(X)<0. If we know the probability density function of variable X as fx(X), the failure probability is evaluated by the integral of the following equation (Faber, 2009).

$$p_f = P\{g(X) < 0\} = \int_{g(x)<0} f_x(X)dx \quad (4)$$

The title of first-order reliability analysis or FORM originally comes from the fact that the value of the importance function g(X) is linearly approximated through Taylor expansion. The integral equation of probabilities is visualized by two dimensions.

Integral simplification is done through transfer by converting the dependent random variable space into a standard space as an independent random variable space. This space including the main variable X=(X1, X2..., Xn) is called X space. In order to convert the integral contours fx(X) into an orderly and symmetrical form, all random variables X=(X1, X2..., Xn) are converted from the X space to the standard space; While the standard variables U=(U_1, U_2, …, U_n) have a specific distribution. In this case, the transformed space is called U space. Finally, the probability integral will be equal to the following equation (Faber, 2009).

$$p_f = \int_{g(u_1.u_2.\dots\ u_n)<0} \dots \int \prod_{i=1}^{n} \frac{1}{\sqrt{2\pi}} \exp\left(-\frac{1}{2}u_i^2\right) d_{u_1} \cdots d_{u_n} \quad (5)$$

Examining the statistical distribution of the data in the figure (4-54) for all the states of the shape parameter i.e. a, shows that the closest fit to this set occurs with the beta probability distribution. Beta continuous distribution has two free parameters on the interval [0 and 1], and these two parameters include α and β. The probability density function of this distribution is given below. The closest fit to our data was obtained around β=1 and α=5.

$$f(x) = \frac{x^{\alpha-1}(1+x)^{-\alpha-\beta}}{B(\alpha.\beta)} \quad (6)$$

Power System Technology
ISSN:1000-3673
Received: 16-01-2024 Revised: 12-02-2024 Accepted: 07-03-2024

In order to further develop the probabilistic integral for evaluation, the form of the function below the integral is simplified; In this case, the boundary integral g(U)=0 will be approximated. For this part, the FORM method uses a linear approximation called the first order analysis of the Taylor expansion in the form of the following equation.

$$g(U) \approx L(U) = g(u^*) + \nabla g(u^*)(U - u^*)^T \quad (7)$$

where L(U) is the linearized importance function, $u^*=(u^*_1, u^*_2, \ldots, u^*_n)$ the design point, T is the basis of transformation and $\nabla g(u^*)$is the slope of the g(U) function at the point u* is The expansion of the significance function is desired at the point that has the highest value of the sub-integral function, which is known as the highest probability density. The point that has the highest probability density in the importance function g(U)=0 is known as Most Probable Point or MPP for short. Mathematical relations to obtain these coordinates will be in the form of the present equation.

The process of FORM calculations is summarized as follows (Faber, 2009).

Transform the original random variable from X-space to U-space using the Rosenblatt transformation.

Searching MPP in U space and calculating the reliability index β.

Reliability calculation $R = \phi(\beta)$.

$$p_f = P\{L(U) < 0\} = \phi\left(\frac{-\mu_L}{\sigma_L}\right) = \phi\left(\frac{\sum_{i=1}^{n} \frac{\partial g}{\partial U_i}\Big|_{u^*} u_i^*}{\sqrt{\sum_{i=1}^{n}\left(\frac{\partial g}{\partial U_i}\Big|_{u^*}\right)^2}}\right) = \phi\left(\sum_{i=1}^{n} \alpha_i u_i^*\right) \quad (8)$$

To investigate the effect of index distribution, depending on the shape parameter, a natural classification with the median limit in the possible limits of the parameter a was used. Therefore, the available values and their equivalent distributions were used to determine the mean values and standard deviation of beta probability distribution. Table (8) shows the summary of statistics (mean and standard deviation) of figure (55) for the data of the new SCS-CN method and based on the classification values of the parameter of figure a (X2). The correlation coefficient is shown in each case with the empirical figure obtained from basic calculations (X1).

Power System Technology
ISSN:1000-3673
Received: 16-01-2024 Revised: 12-02-2024 Accepted: 07-03-2024

Table 8. Shape parameter values in the preparation of performance function variable.

Shape Parameter	R^2	STD (SCS CN*)	Mean (SCS CN*)	STD (SCS CN)	Mean (SCS CN)
a1 = 0.005	0.532	0.072	0.836	0.094	0.95
a2 = 0.2571	0.532	0.064	0.845		
a3 = 0.4632	0.532	0.056	0.854		
a4 = 1.2751	0.527	0.022	0.888		
a5 = 1.989	0.219	-0.035	0.938		
X2				X1	

Using the reliability analysis method, based on the average values and standard deviation specified for the two variables X1 and X2, the IS method was used to discover the uncertainty threshold of changes in the base parameter a. In this way, we were able to evaluate the computational flow rate using the SCS-CN based distribution method probabilistically and based on a performance function.

Considering the dense form of distribution data in a random form of figures, it was preferable to use a sampling method in order to estimate the results more correctly. In statistics, basic importance sampling is a general technique for estimating the properties of a particular distribution, while only generating samples from a distribution different from the underlying distribution. This method was first introduced by Kloek and Dijk in 1978. Various methods can be used to reduce the number of simulations and the coefficient of variation. One of the common methods is the importance sampling (IS) simulation. In the following equation, the information of this approach about the failure level is added to the equation.

$$p_f = p(g(X) \le 0) = \iiint_{g(X)\le 0} I(g(X) \le 0) \frac{f_x(X)}{h_x(X)} h_x(X) dx \quad (4)$$

where $h_x(X)$is the importance sampling probability density function (Faber, 2009). The key to this approach is the selection of $h_x(X)$, so that the samples are mostly obtained from the fracture area. For this reason, a FORM (or SORM) analysis is often performed to find a previous breakpoint (Baker, 2010). which was defined as X2-X1 in our study.

Power System Technology
ISSN:1000-3673
Received: 16-01-2024 Revised: 12-02-2024 Accepted: 07-03-2024

Table 9 summarizes the results of IS-FORM reliability analysis.

Name	DISTRIBUTION ANALYSIS		SIMULATION	
	Number of Simulations	Approximated Number of Bins	Reliability Index Beta	Coefficient of Variation of Pf
a1	30000	83	-0.0915	0.0262
a2			-0.133	0.0289
a3			0.401	0.0418

Conclusion

The results of this research can be summarized in the following cases:

1- Numerical and hydrological models such as HEC-HMS or modelers such as HEC_GeoHMS are completely dependent on the raw DEM layer introduced in order to demarcate upstream.

2- Changes of land cover in flat areas can practically output the closed boundary of the watershed compared to the reality of the land in different simulation models.

3- The single hydrograph method can be a good alternative for areas without rainfall-discharge statistics, considering the basic assumptions such as calibration coefficients.

4- The TUFLOW software model gave the best response to one-dimensional to two-dimensional flow for the city of Vahdita according to the type of boundary conditions.

5- Flood parameters in a hydraulic event model are completely affected by the process of flood hydrograph changes and uncertainty in hydrological calculations is directly transferred to hydraulic models.

6- EO monitoring method in combination with machine learning method can provide accurate classification of land features based on Sentinel-2 satellite images.

7- Prioritizing the flood-prone area using the classification layer of the geological structure will give an effective answer in determining the sensitive areas to the heavy currents.

8- The possibility of climatic changes and the magnitude of the flood flow in events with a larger historical return period is quite probable due to changes in vegetation density.

9- The separation of regions based on flood risk using structural density and the privacy of the flood flow path in the geographic information system environment is dependent on the probability of upstream events for higher flood return periods.

Power System Technology
ISSN:1000-3673
Received: 16-01-2024 Revised: 12-02-2024 Accepted: 07-03-2024

10- Increasing the distance from the river bed has reduced the risk of flooding for possible events, but the density of the structure in the flow path, unlike the occupied area, has an exponential trend.

References

1. Aalbers, E.E., Lenderink, G., van Meijgaard, E., van den Hurk, B.J.J.M., 2018. Local-scale changes in mean and heavy precipitation in Western Europe, climate change or internal variability? Clim. Dyn. 50, 4745–4766. doi.org/10.1007/s00382-017-3901-9.
2. Adger, W.N., 2000. Social and ecological resilience: are they related Prog. Hum. Geogr. 24,3 24, 347–364.
3. Ahn, J.H., Choi, H. Il, 2013. A New Flood Index for Use in Evaluation of Local Flood Severity: A Case Study of Small Ungauged Catchments in Korea. JAWRA J. Am. Water Resour. Assoc. 49, 1–14. doi.org/10.1111/jawr.12025.
4. ARUP International Development, 2012. CITY RESILIENCE INDEX: understanding and measuring city resilience. The Rockefeller Foundation.
5. Azizi, S., Ilderomi, A.R. & Noori, H. Investigating the effects of land use change on flood hydrograph using HEC-HMS hydrologic model (case study: Ekbatan Dam). Nat Hazards 109, 145–160 (2021).
6. Bahadur, A., Pichon, F., 2016. Analysis of Resilience Measurement Frameworks and Approaches. The Resilience Measurement, Evidence and Learning Community of Practice (CoP). Overseas Dev. Institute, London, UK. 54.
7. Bahrami, E., Mohammadrezapour, O., Salarijazi, M. et al. Effect of Base Flow and Rainfall Excess Separation on Runoff Hydrograph Estimation using Gamma Model (Case Study: Jong Catchment). KSCE J Civ Eng 23, 1420–1426 (2019).
8. Baker, Jack. CEE 204: Structrual Reliability. Lecture notes. Stanford University (2010).
9. Balica, S. F., N. Douben, and N. G. Wright. 2009. “Flood vulnerability indices at varying spatial scales.” Water Sci. Technol. 60 (10): 2571–2580. doi.org/10.2166/wst.2009.183.
10. Bartlett, M. S., Parolari, A. J., McDonnell, J. J., and Porporato, A.: Beyond the SCS-CN method: A theoretical framework for spatially lumped rainfall-runoff response, Water Resour. Res., 52, 4608–4627, (2016a).
11. Bartlett, M. S., Parolari, A. J., McDonnell, J. J., and Porporato, A.: Framework for event-based semidistributed modeling that unifies the SCS-CN method, VIC, PDM, and TOPMODEL, Water Resour. Res., 52, 7036–7052, (2016b).
12. Batica, J. Methodology for flood resilience assessment in urban environments and mitigation strategy development. 2015.tel.archives-ouvertes.fr/tel-01159935.

Power System Technology
ISSN:1000-3673
Received: 16-01-2024 Revised: 12-02-2024 Accepted: 07-03-2024

13. Batica, J., Gourbesville, P., 2016. Resilience in Flood Risk Management - A 504 New Communication Tool. Procedia Eng. 154, 811–817. doi.org/10.1016/j.proeng.2016.07.411.
14. Beven, K.: Rainfall-Runoff Modelling: The Primer, 2nd Edn., Wiley-Blackwell, Chichester, UK, (2012).
15. Blackmore, J., and R. Plant. 2008. "Risk and resilience to enhance sustainability with application to urban water systems." J. Water Resour. Plann. Manage. 134 (3): 224–233. doi.org/10.1061/(ASCE) 0733-9496(2008) 134:3(224).
16. Blanc, J., Hall, J.W., Roche, N., Dawson, R.J., Cesses, Y., Burton, A., et al., 2012. Enhanced efficiency of pluvial flood risk estimation in urban areas using spatial–temporal rainfall simulations. J. Flood Risk Manage. 5, 143–152.
17. Bras, R. L.: Hydrology: an introduction to hydrologic science, Addison Wesley Publishing Company, Reading, MA, (1990).
18. Bruneau, M., Eeri, M., Chang, S.E., Eeri, M., Ronald, T., Eeri, M., Lee, G.C., Eeri, M., Rourke, T.D.O., Eeri, M., Reinhorn, A.M., Eeri, M., Shinozuka, M., Eeri, M., Wallace, W.A., Winterfeldt, D. Von, 2003. A Framework to Quantitatively Assess and Enhance the Seismic Resilience of Communities 19, 733–752. doi.org/10.1193/1.1623497.
19. Burian, S. J., and F. G. Edwards. 2002. "Historical perspectives of urban drainage." In Proc., 9th Int. Conf. on Urban Drainage. London: International Association for Hydro-Environment Engineering and Research, Madrid and International Water Association.
20. Centre for Research on the Epidemiology of Disasters (CRED), United Nations Office for Disaster Risk Reduction (UNISDR), 2015. The human costs of weather related disasters 1995-2015. Centre for Research on the Epidemiology of Disasters (CRED); United Nations Office for Disaster Risk Reduction (UNISDR).
21. Dong, X., Guo, H., Zeng, S., 2017. Enhancing future resilience in urban drainage system: Green versus grey infrastructure. Water Res. 124, 280–289. doi.org/10.1016/j.watres.2017.07.038.